Nano Today 28 (2019) 100763

Contents lists available at ScienceDirect

Nano Today

journal homepage: www.elsevier.com/locate/nanotoday

Review

State-of-the-art progress in the use of ternary metal oxides as photoelectrode materials for water splitting and organic synthesis

Huichao He[a,1], Aizhen Liao[c,1], Wenlong Guo[b], Wenjun Luo[c], Yong Zhou[c,*], Zhigang Zou[c]

[a] State Key Laboratory of Environmental-Friendly Energy Materials, School of Materials Science and Engineering, Southwest University of Science and Technology, Mianyang 621010, China
[b] Chongqing Key Laboratory of Green Synthesis and Applications, College of Chemistry, Chongqing Normal University, Chongqing 401331, China
[c] Ecomaterials and Renewable Energy Research Center, School of Physics, Nanjing University, Nanjing 211102, China

ARTICLE INFO

Article history:
Received 26 January 2019
Received in revised form 10 June 2019
Accepted 13 August 2019
Available online 23 August 2019

Keywords:
Ternary metal oxides
Photoelectrochemical water splitting
Photoelectrochemical organic synthesis

ABSTRACT

To tackle the issue of the depletion of fossil fuels and their environmental misdeeds, photoelectrochemical (PEC) water splitting and organic synthesis have been drawing increasing attention as promising environmentally friendly approaches for the production of hydrogen fuel and organics. In the past few decades, almost all possible binary metal oxide semiconductors have been investigated as photoelectrode materials for PEC applications; however, a satisfactory photoelectrode remains elusive. As a result, ternary metal oxide semiconductors have garnered worldwide attention in recent years as potential photoelectrode materials due to their unique advantages. In this review, we firstly introduced the fundamental properties and limitations of ternary metal oxide semiconductors for PEC water splitting and organic synthesis. Then, modified strategies for the performance of ternary metal oxide photoelectrodes are highlighted. Next, recent developments in the use of ternary metal oxide semiconductors as photoelectrode materials for water splitting and organic synthesis are summarized. Finally, several perspectives are presented with respect to the future outlook of PEC water splitting and organic synthesis using ternary metal oxide photoelectrodes. This review provides a systematic overview of the developing information and a referential direction for this research field.

Contents

* Corresponding author.
E-mail address: zhouyong1999@nju.edu.cn (Y. Zhou).
[1] He and Liao contributed to this work equally.

https://doi.org/10.1016/j.nantod.2019.100763
1748-0132/

Introduction

Solar energy is a fundamental energy supporting the sustainable development of human society and the ecological environment. Quantitatively, the potentially available sunlight power reaching the Earth's surface is estimated to be around 8.6×10^4 TW/year [1], which is much higher than the global energy consumption of human activities in 2018 (about 19 TW) [2]. In recent decades, several solar-utilization technologies (such as photovoltaic technology [3,4], photocatalysis technology [5,6], and solar-thermal technology [7]) have been developed and studied in order to address environmental pollution issues and fossil fuel shortages. Among these solar-utilization technologies, photoelectrochemical (PEC) water splitting and organic synthesis are considered to be promising environmentally friendly approaches for the production of hydrogen fuel and organics [5,8]. From the perspective of energy conversion, solar energy can be converted into hydrogen fuel or chemical energy of organics through semiconductor photoelectrodes during water splitting or organic synthesis reactions.

PEC water splitting and organic synthesis are both initiated with the photo-induced charge of semiconductor electrodes under solar illumination [8,9]. Taking water splitting in an n-type semiconductor-based PEC cell as an example, the PEC water splitting step can be generalized as follows (shown in Fig. 1a). (i) Electrons and holes are respectively generated in the conduction and valance band of the n-type semiconductor electrode when it absorbs photons with higher energy than its band gap. (ii) If the valence band edge of the n-type semiconductor is higher than the water oxidation potential (1.23 V *vs.* RHE), the water molecules will be split into oxygen molecules on the n-type photoelectrode via the theoretical oxidative ability of photo-induced holes. (iii) Meanwhile, the electrons of the n-type photoelectrode are directionally transferred to the counter electrode via bias driving through the outer circuit. When the conduction band edge of the n-type semiconductor or the applied bias on the counter electrode is lower than the proton reduction potential (0 V *vs.* RHE), the water molecules or protons are theoretically reduced into hydrogen on the counter electrode. In the case of p-type semiconductor-based PEC cells, the water molecules or protons are photoelectrochemically reduced into hydrogen on the surface of the p-type photoelectrode, while the water molecules are oxidized into oxygen on the counter electrode via photo-excited holes (shown as Fig. 1b). In addition, the water molecules could be reduced and oxidized simultaneously in a tandem system composed of an appropriate n-type photoelectrode and a p-type photoelectrode (see Fig. 1c). On the whole, the fundamental principles of PEC organic synthesis are similar to PEC water splitting. In essence, both of them involve solar-driven oxidation or reduction reactions on semiconductor electrodes [8,10].

For PEC water splitting or organic synthesis, the semiconductor electrode is the heart of the PEC system; thus, its performance has a fundamental influence on the efficiency of the water splitting and organic synthesis reactions. It is generally accepted that an effective PEC reaction involves seamless cooperation between light harvesting, charge separation, and the surface reaction of the semiconductor electrode [11–13]. With consideration for the integral PEC reaction process, the ideal semiconductor electrode for PEC water splitting or organic synthesis should exhibit the following properties: (i) suitable band gap for wide absorption of solar light; (ii) modest band edge position to straddle a specific oxidation or reduction reaction potential; (iii) satisfactory PEC reaction stability in electrolytes; (iv) high charge transfer and separation efficiency as well as fast PEC kinetic reaction; and (v) acceptable production cost and abundance of raw materials. In the past few decades, almost all possible binary metal oxide semiconductors have been investigated as photoelectrode materials for PEC applications [14,15]; however, a satisfactory photoelectrode remains elusive. As a result, ternary metal oxide semiconductors have garnered worldwide attention as potential photoelectrode materials due to their unique advantages. Ternary metal oxides offer a variety of suitable band gaps and modest band edge positions to potentially achieve high PEC efficiency [16,17]. Further, the various possible combinations of ternary metal oxides increase the likelihood of finding a desirable photoelectrode material for PEC applications.

The research on ternary metal oxide photoelectrodes for PEC water splitting and organic synthesis has developed rapidly in recent years. Therefore, it is an appropriate time to summarize the periodical progress of ternary metal oxide photoelectrodes for PEC water splitting and organic synthesis, with the intention of providing a systematic overview of the developing information and a referential direction for this research field. This review firstly introduces the fundamental properties and limitations of ternary metal oxide semiconductors for PEC water splitting and organic synthesis. Then, modified strategies for the PEC performance of ternary metal oxide photoelectrodes are highlighted. Next, recent developments in the use of ternary metal oxide semiconductors as photoelectrode materials for water splitting and organic synthesis are summarized. Finally, several perspectives are presented with respect to the future outlook of PEC water splitting and organic synthesis using ternary metal oxide photoelectrodes.

Fundamental properties and limitations of ternary metal oxide photoelectrodes

Band gap and structure features of ternary metal oxides

On the Earth's surface, the proportion of visible light energy (400 nm< λ <800 nm) in the solar spectrum is close to 50%; it is essential to utilize the visible light energy for large-scale PEC applications. For example, a solar-to-hydrogen (STH) efficiency of 10% and a stability of 1000 h are generally considered to be the minimum threshold for the commercial application of PEC water splitting [18,19]. To attain such performance in the PEC water splitting reaction, the semiconductor electrodes in the PEC cell should provide at least ~1.6 V holes potential (1.23 V and overpotential) and a photocurrent density of 8.2 mA/cm^2 [20]. Ternary metal oxide semiconductors are an intriguing material class; there is a large quantity of potential ternary metal oxide semiconductors that may possess the desired optical properties and band structure for PEC water splitting and organic synthesis. In general, the valence band of most ternary metal oxide semiconductors is composed of a hybridization of O 2p orbital with a d^0 or d^{10} orbital of one metal cation [16]. The other metal cation in ternary metal oxide provides an orbital for the constitution of its conduction band. Due to the hybridization of the O 2p orbital with the metal element orbital, the valence bands of ternary metal oxides are pushed upward and their band gaps are decreased slightly relative to binary metal oxides. An example is $BiVO_4$ which has a band gap of ~2.4 eV [21,22]; its valence band consists of the hybridization of O 2p orbital with Bi 6 s orbital. The valence band edge of $BiVO_4$ is slightly pushed upward relative to Bi_2O_3 (~2.7 eV) [23]. Accordingly, ternary metal oxide semiconductors can offer a variety of required band gap energies for PEC reactions. As shown in Fig. 2, several typical ternary metal oxides have been demonstrated to have a band gap energy in the range of 1.6–2.3 eV, which could theoretically achieve over 10% STH efficiency in a PEC water splitting device.

Performance limitations and application challenges of ternary metal oxide photoelectrodes

Although ternary metal oxides have several advantages as photoelectrode materials, the actual performance of ternary metal

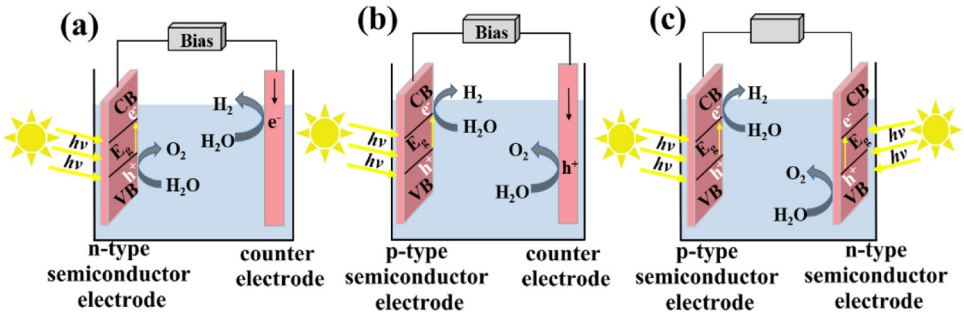

Fig. 1. PEC water splitting in (a) n-type semiconductor-based PEC system, (b) p-type semiconductor-based PEC system, and (c) tandem system.

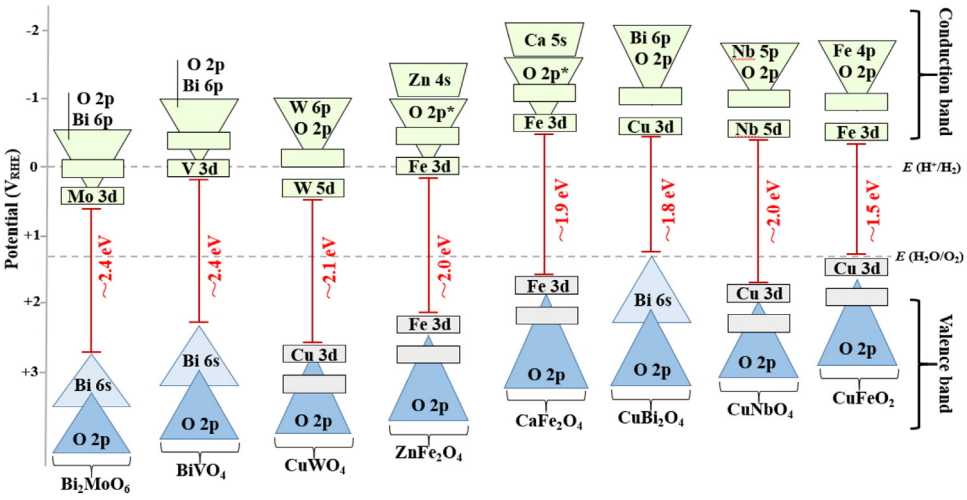

Fig. 2. The band structure of several typical ternary metal oxide semiconductors.

oxide photoelectrodes are unfortunately affected by several limitations. First, the charge transfer and separation properties of most of ternary metal oxide photoelectrodes are unsatisfactory. As mentioned above, the valence band of ternary metal oxide semiconductors consists of hybrid orbitals; empty metal orbitals normally arise in their band structure. These empty orbitals of metal cations usually result in carrier localization and low carrier mobility [24,25]. The poor charge transfer and separation properties naturally hamper the PEC activity of ternary metal oxide photoelectrodes. Second, the PEC kinetics on most of ternary metal oxide photoelectrodes is too sluggish to high performance. The PEC reactions on photoelectrodes (such as, water splitting reaction) normally involve multistep proton-coupled electron transfer process, but the inactive conductivity and hydrophily of ternary metal oxides cannot provide sufficient support for PEC reactions. Three, the stability of ternary metal oxide photoelectrodes in the present does not reach the requirement of PEC applications. On the face of it, the unsatisfactory stability of ternary metal oxide photoelectrodes is originated from their dissolution in aqueous solution. In essence, the dissolution of ternary metal oxide photoelectrodes is mainly caused by their poor charge transfer and separation properties as well as sluggish kinetics for reactions, which jointly induce the photocorrosion of ternary metal oxides [26].

For the PEC applications of ternary metal oxide photoelectrodes, the first challenge is screening out the ternary metal oxides with high-performance. In theory, the amount of possible ternary metal oxides is vast. At present, the efficient approaches for the experimental screening and theoretical prediction of desired ternary metal oxides are inadequate though some efforts have been initiated. Second, the accurate and facile synthesis of ternary metal oxide photoelectrodes is also challenging. Stoichiometry of metal cations and oxygen has an obvious influence on the PEC performance of ternary metal oxides [27,28]. The synthesis of ternary metal oxides is highly reliant on harsh conditions in particular at high temperature, which may lead to selective loss of one of the metal elements due to differences in the metal cation vapor pressure [29]. The minor sub-stoichiometry of metal cations could induce a high concentration of defects in ternary metal oxides [30], which may act as recombination centres of charge carrier, naturally impacting on the performance of the photoelectrodes. To date, the accurate and facile synthesis of ternary metal oxide photoelectrodes remains a bottleneck that restricts the systematic investigation of these photoelectrons as well as their large-scale application prospects.

Modified strategies for the performance of ternary metal oxide photoelectrodes

As described in the above sections, ternary metal oxides have distinctive features that make them highly promising photoelectrode materials for PEC water splitting and organic synthesis. However, the typical photon-to-product conversion efficiency of most ternary metal oxide photoelectrodes is far below the theoretical expectations due to several identified performance limitations. Numerous attempts have been made to address one or more of these performance issues with varying degrees of success; such attempts include composition or morphology-tuning, coupling of a co-catalyst or photocatalyst, and crystal facet-engineering. In this section, an overview of these types of modifications on the PEC performance of ternary metal oxide photoelectrodes is provided, and the relevant findings are discussed.

Composition or morphology-tuning

Previous experimental investigations and theoretical calculations have revealed that both the composition and morphology of a photoelectrode have a significant influence on its light harvesting, charge transfer and separation, and the surface reaction efficiency [31,32]. Specifically, the band gap, band edge position, carrier transport property, and surface reaction kinetics of a photoelectrode are highly related to its composition. Meanwhile, the morphological characteristics of a photoelectrode, such as its thickness, size, and shape, affects its light absorption intensity, charge separation efficiency, and surface reaction kinetics. For a specific ternary metal oxide, the bulk carrier-diffusion length, band gap, and band edge position are nearly constant. The charge collection efficiency on the surface of a ternary metal oxide photoelectrode could be optimized when the thickness and dimensions of the photoelectrode are in the same range as its carrier-diffusion length. In addition, the electrical and optical properties as well as depletion region of a photoelectrode are more favorable for PEC reactions when the ternary metal oxide is incorporated with suitable dopants or oxygen vacancies. Therefore, composition alterations and morphology-tuning of ternary metal oxide photoelectrodes are two effective and common ways to improve their PEC performance. Several typical composition or morphology-tuning works that have been recently reported to modify the PEC performance of ternary metal oxide photoelectrodes are reviewed below.

It has been reported that the transport of charge carrier in many metal oxides is based on a small polaron hopping conduction mechanism [24,25,33]. Such a polaron conduction mechanism usually results in relatively low charge carrier mobility in ternary metal oxide semiconductors. Suitable metal-impurity doping is expected to modify the charge localization of ternary metal oxides, improving their charge carrier mobility during PEC reactions. In the work of Bard's group [34], various metals (W, Fe, B, Cu, Zn, Ti, Nb, Sn, Co, Pb, Rb, Ru, Ag, Ga, Sr, and Ir) were investigated as dopants to improve the PEC activity of $BiVO_4$ via a scanning electrochemical microscopy (SECM) technique. The doping effects were quickly and intuitively screened based on the SECM image of $BiVO_4$-based arrays, and were further examined on larger $BiVO_4$-based film photoelectrodes by means of PEC measurements. This work indicated that the co-doping of 2% W and 6% Mo resulted in the most effective enhancement of the PEC activity of $BiVO_4$, without a significant influence on the band gap of $BiVO_4$. Similar results were subsequently observed in the work of Luo et al. [35], and have subsequently been replicated in several theoretical calculations and experimental studies [36–38]. W and Mo both have 6 valence electrons; the substitution of the partial sites of V^{5+} in $BiVO_4$ can lead to donor-doped $BiVO_4$ with improved bulk electron-hole transfer efficiency and higher conductivity [34,39]. Additionally, proper metal substitutes the partial sites of Bi^{3+} in $BiVO_4$, having a positive effect on the PEC activity of $BiVO_4$ photoanodes. Zhang *et. al.* reported that higher PEC activity was obtained with a Y^{3+}-doped $BiVO_4$ film photoelectrode by means of Y^{3+} substitution in the partial sites of Bi^{3+} in $BiVO_4$ [40]. Our recent work observed that In^{3+} substituting the partial sites of Bi^{3+} in $BiVO_4$ does not obviously change the band gap of $BiVO_4$, but results in higher surface-charge separation efficiency for PEC water oxidation. Both experimental and theoretical calculation outcomes have revealed that In^{3+}-doping passivates the surface states of $BiVO_4$, thus inhibiting the nonradiative recombination of surface charge [41].

Significantly, there is a vast amount of potential metal-doped ternary metal oxides; however, methods for rapid screening and identification of effective ternary metal oxides as photoelectrode materials are less advanced. The SECM technique reported by Bard et al. provides an effective method for experimentally screening possible metal-doped ternary metal oxides as photoelectrode materials [34,42]. In subsequent work, Zn and Ag were screened by the SECM technique and were found to be effective dopants for improving the PEC activity of Bi_2WO_6 (12% Zn-Bi_2WO_6) and $CuBi_2O_4$ (10% Ag-$CuBi_2O_4$) photoelectrodes [43,44]. In recent years, the research of high-throughput methods for screening photocatalysts has drawn attention [45,46], which could provide approach references to select ternary metal oxides as photoelectrode materials. For example, Gao and co-worker reported combinatorial approaches to screen ABO_3-type oxides (A = Y, La, Nd, Sm, Eu, Gd, Dy, Yb; b = Al and In) as photocatalysts [47]. From their investigations, $YInO_3$ and $YAlO_3$ were identified to be the optimal photocatalysts since the $YInO_3$ and $YAlO_3$ spots with methylene blue solution show noticeable color change before and after sunlight irradiation. Zhang *et. al* applied microfluidic chip-based analytical system for rapid screening of metal-doped TiO_2 photocatalysts [48]. In addition, theoretical calculation methods were developed to predict and screen photocatalysts. In the work of Ceder et al., first principles calculation was used as high throughput approach to screen nitrides and oxynitrides for solar water-splitting [49]. Zhou *at. al* reported the computational screening of 2D materials and rational design of heterojunctions as photocatalysts for water splitting [50]. For the quick find of ternary metal oxide photoelectrodes with high-performance, it is necessary to build a database of ternary metal oxide photocatalysts through the combination of experimental and computational screening.

In general, metal doping is a frequently used strategy to modify the PEC activity of ternary metal oxide photoelectrodes. Nakatsuj et al. reported Rh-doped $SrTiO_3$ photocathodes has higher hydrogen-producing efficiency than the undoped $SrTiO_3$ photocathodes [51]. The study by Bohra et al. indicated that a 0.3% Fe-doped $CuWO_4$ photoanode exhibited 1.5 times the photocurrent density and 50% greater charge separation efficiency for water oxidation compared to an undoped $CuWO_4$ photoanode at 1.23 V vs. RHE [52]. Our previous work revealed that a 5% Ti-doped $BiFeO_3$ photoanode exhibited a higher charge carrier concentration for water oxidation than an undoped $BiFeO_3$ photoanode [53]. Ti-doped $ZnFe_2O_4$ has been demonstrated to be a better photoanode material for PEC water splitting relative to the pristine $ZnFe_2O_4$ [54].

Nonmetal doping has also been developed as an effective composition-tuning strategy to modify the electronic and optical properties of ternary metal oxide semiconductors. It is well known that O *2p* orbitals lay relatively lower than C *2p*, S *2p*, N *2p,* and P *2p* orbitals on the energy scale. Once the oxygen sites are partially substituted with non-metal anions with higher energy orbitals, the valance band of ternary metal oxides can potentially be pushed upward, decreasing the band gap of the photoelectrode. In their theoretical calculation work, Piskunov et al. used first-principles calculations to predict that sulfur-doped $SrTiO_3$ nanotubes are of a visible-light-response band distribution for the oxygen evolution reaction [55]. Similarly, sulfur-doped $ZnIr_2O_4$ [56], nitrogen-doped Bi_2WO_4 [57], nitrogen-doped $BiVO_4$ [58], and nitrogen-doped $ZnGa_2O_4$ [59] have been predicted to possess narrower band gap according to the investigations of theoretical calculation. In experimental research, the band gaps of sulfur-doped ZrW_2O_8 [60], nitrogen-doped ZnCaOx [61], nitrogen-doped $Ba_5Ta_3O_{15}$, [62], and nitrogen-doped $SrTiO_3$ [63] have been demonstrated to be narrower than their undoped counterparts. In the study by Jo et al. [64], phosphorus-doped $BiVO_4$ was evaluated for its potential as a higher activity photoanode material for water oxidation. A urea-precipitation method was used to synthesize the phosphorus-doped $BiVO_4$, in which a small fraction of VO_4^{3-} oxoanions were replaced by PO_4^{3-} oxoanions in the precursor solution. This study found that phosphorus doping into $BiVO_4$ induces a slight change in the band gap energy of $BiVO_4$ (0.01-0.04 eV), but results in a significant enhance-

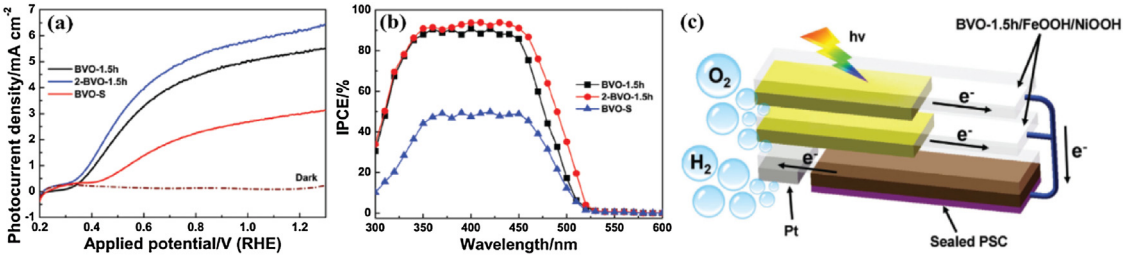

Fig. 3. (a) Photocurrent density versus applied potential curves, (b) IPCE curves at 1.23 V versus RHE of the BVO-1.5 h (with oxygen-vacancies), 2-BVO-1.5 h (with oxygen-vacancies), and BVO-S (without oxygen-vacancies) films. (c) Schematic of the 2-BVO-1.5/FeOOH/NiOOH dual photoanodes coupled with a sealed perovskite solar cell (PSC). Reprinted by permission from *Ref.* [69], Copyright of 2018, Wiley-VCH.

ment in its PEC water oxidation activity; $Bi(VO_4)_{0.995}(PO_4)_{0.005}$ exhibited the best PEC water oxidation activity. Further electrochemical impedance spectroscopy measurements and density functional theory (DFT) calculations revealed that the charge transfer resistance of the $BiVO_4$ photoanode was remarkably reduced by phosphorus-doping, and the lattice strain induced by phosphorus-doping could be advantageous for the separation of electron-hole pairs. Additionally, fluorine-doped $BiVO_4$ has been investigated as a higher activity photoanode material for water oxidation [65].

Another typical composition-tuning strategy for the modification of ternary metal oxide photoelectrodes is the introduction of oxygen vacancies. The concept and function of introducing oxygen vacancies was initially demonstrated in binary metal oxide photocatalysts (such as TiO_2, WO_3, and Fe_2O_3) [66]. Oxygen vacancies are typical intrinsic defects that have an obvious influence on the electronic and optical properties of transition metal oxides via the manipulation of their donor density [67]. In light of the success of oxygen vacancies in binary metal oxide photocatalysts, a number of studies have been focused on the ternary metal oxide photoelectrodes with oxygen vacancies. Li et al. reported that hydrogen-treated $BiVO_4$ films exhibit significantly enhanced activity and stability for PEC water oxidation due to the formation of oxygen vacancies and hydrogen impurities [68]. In the study by Wang and co-workers, $BiVO_4$ films with well-controlled oxygen vacancies were prepared via an electrodeposition process with a mild thermal treatment process [69]. Since the enriched oxygen vacancies can act as shallow donors in $BiVO_4$, the optimized $BiVO_4$ film with oxygen vacancies showed a high photocurrent density of 6.22 mA cm^{-2} at 1.23 V *vs.* RHE in Na_2SO_3-containing solution under AM 1.5 G illumination. Based on the $BiVO_4$ film with optimized content of oxygen vacancies, a high solar-to-hydrogen conversion efficiency of 6.5% for unbiased water splitting was achieved on an artificial leaf that consisted of $BiVO_4$/FeOOH/NiOOH dual photoanodes and a single sealed perovskite solar cell (shown in Fig. 3). Similar enhancement of PEC activity and stability on oxygen vacancies-containing $BiVO_4$ films has also been reported in other studies [70–72]. In addition, several other ternary metal oxides with oxygen vacancies (such as $CuWO_4$ [73–75] and $ZnFe_2O_4$ [76,77]) have been demonstrated to be better photoelectrode materials for PEC reactions. Notably, compared to metal-doping and nonmetal-doping, the introduction of oxygen vacancies could improve the PEC activity and stability of ternary metal oxide photoelectrodes simultaneously.

Empirically, the PEC reaction efficiency (η) of photoelectrodes is mainly influenced by the following three factors [11–13]: (i) the light harvesting efficiency of the semiconductor electrode (η_{abs}); (ii) the charge separation efficiency of the semiconductor electrode (η_{sep}); and (iii) the charge injection efficiency of the semiconductor electrode/electrolyte interface (η_{inj}). The practical PEC reaction on photoelectrodes can be expressed as in Eq. (1):

$$\eta = \eta_{abs} \times \eta_{sep} \times \eta_{inj} \quad (1)$$

It is commonly recognized that photoelectrodes with a nanostructure are physically favorable to the PEC reaction. Nanostructured photoelectrodes not only have a high surface area for the PEC reaction, but also have enhanced capabilities in terms of light harvesting, charge separation, and collection. Tuning the morphology of ternary metal oxides with low carrier mobility and sluggish PEC kinetics to an optimized nanostructure could improve their PEC performance.

To alleviate the inefficient charge separation of $CuWO_4$ photoelectrodes, Ye et al. designed and prepared a $CuWO_4$ nanoflake array film on FTO glass that showed an anodic current density of ~0.4 mA/cm^2 in potassium borate buffer [78]. The photocurrent achieved on their $CuWO_4$ nanoflake array film was higher than all previously available bare $CuWO_4$ films. Additionally, the PEC activity of the $CuWO_4$ nanoflake array film could be further improved up to 2 mA/cm^2 by taking advantage of its high surface area and abundant porosity to couplie with $BiVO_4$ and Ni nanoparticles (see Fig. 4). In other work related to $CuWO_4$ photoelectrodes [78,79], nanostructured $CuWO_4$ films were demonstrated to exhibit higher PEC performance and were more favorable for the construction of $CuWO_4$-based photoelectrodes. In the work of Zhou et al. [80], 3D nano-flowerlike $CuWO_4$ film was prepared on an FTO glass substrate via the hydrothermal method; this film exhibited a photocurrent density of 0.58 mA/cm^2 for PEC water oxidation at 0.8 V versus RHE in 0.1 Na_2SO_4. On the basis of this 3D nanostructure, CdS and FeOOH nano-layers were further coupled with the $CuWO_4$ nanoflower film. The triple $CuWO_4$/CdS/FeOOH photoanode showed a higher photocurrent density of about 2.05 mA/cm^2 at 0.8 V versus RHE as well as excellent operation stability due to its heterojunction configuration.

Similarly, superior PEC activity has been observed on a series of nanostructured ternary metal oxide photoelectrodes, including Bi_2WO_6 [81], $ZnFe_2O_4$ [82,83], NiV_2O_6 [84], and $BiVO_4$ [85–87]. It is noteworthy that the preparation of nanostructured ternary metal oxide film is more difficult than binary metal oxide film due to the thermodynamic difficulty of nucleation on the substrate. At present, the template-induced method is the most common method for the preparation of nanostructured ternary metal oxide films. For example, nanostructured WO_3 film has commonly been used as a template for the preparation of nanostructured $CuWO_4$ film [78,79], while nanostructured FeOOH and BiOI act as common templates for the preparation of nanostructured $ZnFe_2O_4$ and $BiVO_4$ films [82,83,86], respectively. Other methods such as reactive ballistic deposition [85] and chemical vapor deposition (CVD) [88,89] usually rely on relatively complicated procedures and conditions for the preparation of nanostructured ternary metal oxide films. Therefore, the development of a facile and universal method for the preparation of nanostructured ternary metal oxide films is critical. In our previous work, polyethylene glycol 600 was found to be an effective structure-directing agent that functions to optimize the structure of $BiVO_4$ and W/Mo-doped $BiVO_4$ films. Accordingly, a simple drop-casting method was developed for the preparation

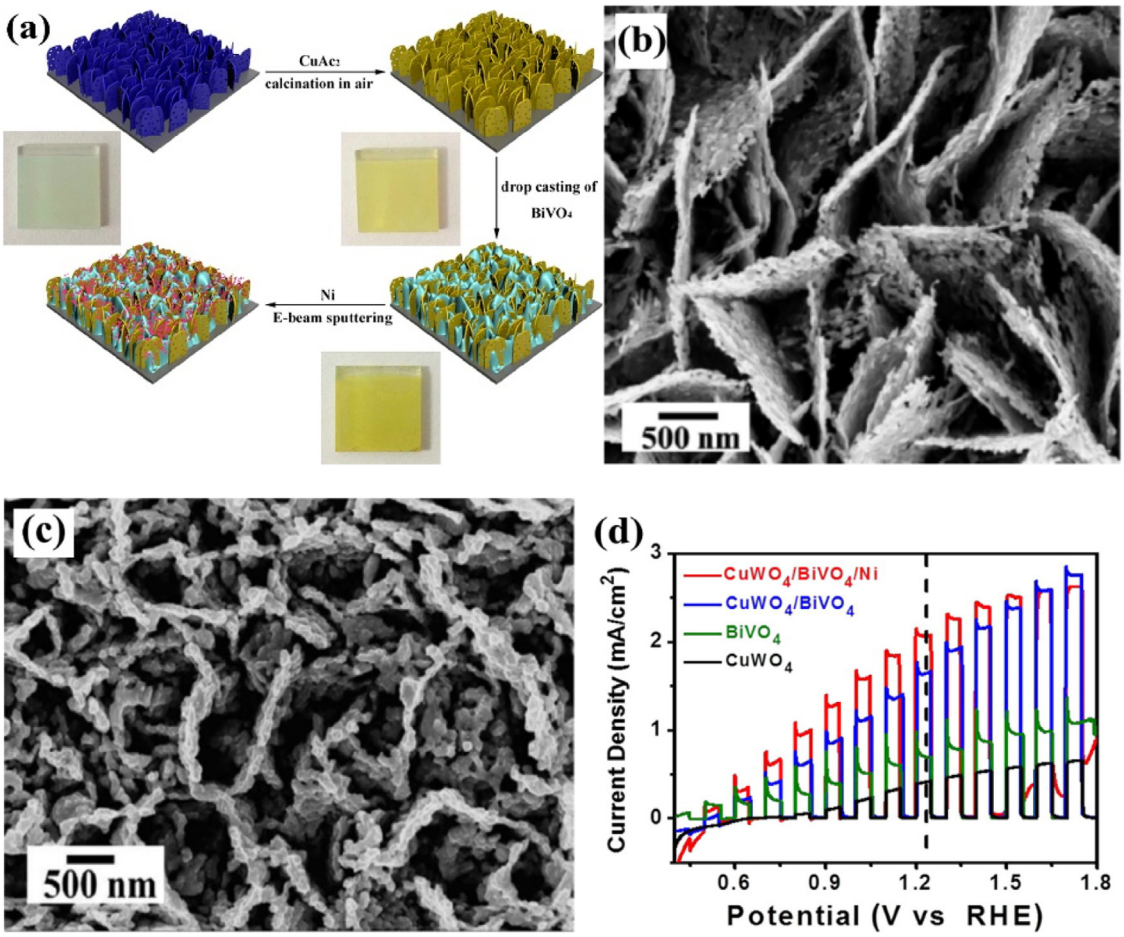

Fig. 4. (a) Schematic illustration of the conversion process from WO_3 nanoflake arrays to $CuWO_4$ nanoflake arrays, $CuWO_4/BiVO_4$ heterojunction and $CuWO_4/BiVO_4$/Ni on the FTO glass. SEM image of (b) $CuWO_4$ nanoflake arrays and (c) $CuWO_4/BiVO_4$ heterojunction film on the FTO glass. (d) Linear sweep voltammetry curves of $CuWO_4$, $BiVO_4$, CuWO4/$BiVO_4$ and $CuWO_4/BiVO_4$/Ni films under chopped illumination. Reprinted by permission from *Ref.* [78], Copyright of 2016, the American Chemical Society.

of undoped and W/Mo-doped $BiVO_4$ nanoflake array films [87]. Zhang et al. reported a hydrothermal anion exchange method for the preparation of porous nanoflake BiMOx (M = W, V, and Mo) photoanodes [90]. In their synthesis process, BiOI film was used as the universal template and Bi source, and was eventually converted to a Bi-based porous nanoflake film upon reaction with MOx (M = W, V, and Mo)-containing precursors.

In PEC reactions, the separation and delivery of charge carrier largely relies on the depletion region formed at the photoelectrodes/electrolyte interface through the band bending [91]. The depletion region of photoelectrodes is usually in the range of 20–100 nm [92,93], which could be manipulated by the impurities doping and surface morphology controlling. In previous works, graded doping has been demonstrated to be capable of improving the PEC activity of ternary metal oxide photoelectrodes through widening their depletion region. Typically, Liu *et. al* found that the depletion region of n-$SrTiO_3$ photoanodes were widened by heavily doped with oxygen vacancies in bulk of $SrTiO_3$ and lightly doped on their surface [94]. The n-$SrTiO_3$ photoanodes with graded oxygen vacancies show obviously improved solar water splitting activity. Similar change of depletion region was observed in Ir doped n-$SrTiO_3$ photoelectrodes, Co-doped and Zn-doped $BiVO_4$ photoanodes [51,95,96]. In addition, tuning the surface morphology of ternary metal oxide nanocrystal have been used to manipulate their depletion region for PEC reactions. In the work of Krtil and coworkers, the PEC water splitting activity of $SrTiO_3$ nano-cubes has been reported to be closely related to their size due to the change of depletion region [97].

Coupling of co-catalysts or photocatalysts

Efficient bulk and surface charge separation and transfer are critical for the PEC reaction of photoelectrodes. The efficiency of surface charge separation and transfer is interconnected with the PEC reaction kinetics and stability of the photoelectrodes [20]. Unfortunately, the surface charge separation and transfer properties, as well as the PEC reaction kinetics, of most ternary metal oxide photoelectrodes fall short of the requirements of efficient PEC water splitting and organic synthesis [16]. Proper oxygen or hydrogen evolution catalysts coupled with ternary metal oxides have demonstrated effective improvement in the PEC water splitting kinetics of ternary metal oxide photoelectrodes. Since the oxygen or hydrogen evolution catalysts have abundant active sites for the water splitting reaction [98], the water splitting overpotential of ternary metal oxide photoelectrodes could be reduced through the synergistic reaction with co-catalysts. In theory, once the photogenerated charge of a ternary metal oxide photoelectrode is consumed by the water splitting reaction quickly, the accumulation of charge on the photoelectrode will decrease. As a result, the photocorrosion of photoelectrode will be kinetically suppressed, and simultaneous enhancement in the PEC reaction stability and activity could be achieved [26]. Additionally, constructing proper ternary metal oxide/photocatalyst heterojunction has function of improving the activity and stability of ternary metal oxide photoelectrodes. The enhancement of PEC performance of ternary metal oxide/photocatalyst heterojunction photoelectrodes is mainly attributed to the band matching effect. The surface charge

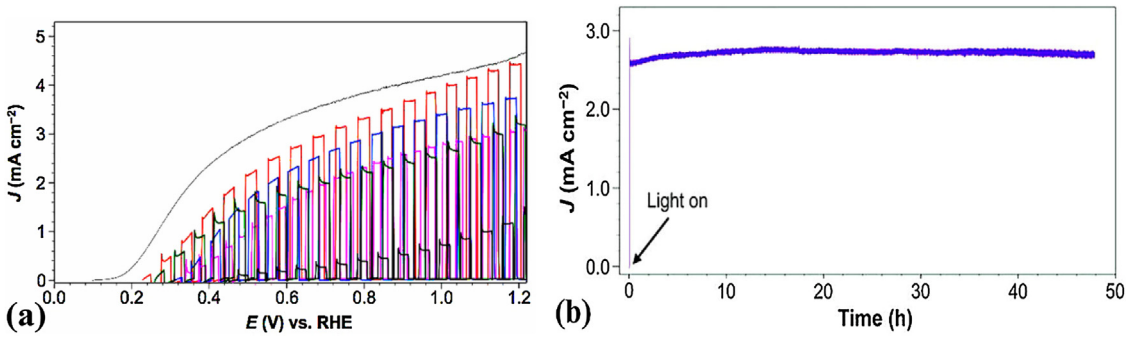

Fig. 5. (a) J–V curves of $BiVO_4$ (black solid), $BiVO_4$/FeOOH (blue), $BiVO_4$/NiOOH (green), $BiVO_4$/FeOOH/NiOOH (red), $BiVO_4$/NiOOH/FeOOH (pink) for water oxidation and $BiVO_4$ for sulfite oxidation (gray); (b) *J*-t curve of $BiVO_4$/FeOOH/NiOOH photoanode measured at 0.6 V versus counter electrode. All characterizations were performed in 0.5 M phosphate buffer (pH 7) under AM 1.5 G illumination. Reprinted by permission from *Ref.* [100], Copyright of 2014, American Association for the Advancement of Science.

separation and transfer of heterojunction photoelectrodes can be directionally induced from the ternary metal oxide to the photocatalyst through the potential differences in their conduction band and valence band.

In recent years, transition metal-based oxide/hydroxides (such as Co, Ni, and Fe-based oxides/hydroxides) have been identified to be efficient co-catalysts for improving the PEC performance of ternary metal oxide photoelectrodes [99]. Choi and co-workers found that FeOOH and NiOOH-coupled $BiVO_4$ have superior PEC water oxidation activity than $BiVO_4$ [100]. Their results indicated that the water oxidation activity on the coupled $BiVO_4$ photoanodes obeys the following sequence: $BiVO_4$/FeOOH/NiOOH > $BiVO_4$/FeOOH > $BiVO_4$/NiOOH/FeOOH≈ $BiVO_4$/NiOOH (see Fig. 5a). Furthermore, they demonstrated that the interface charge recombination of $BiVO_4$/FeOOH was reduced, and the Helmholtz layer potential drop (V_H) of $BiVO_4$/NiOOH was decreased to achieve faster water oxidation kinetics. Accordingly, the $BiVO_4$/FeOOH/NiOOH photoanodes exhibited long-term stability and high activity for solar water oxidation, which were maintained for 48 h without showing any sign of decay (Fig. 5b). Similar improvements in PEC water oxidation activity have also been observed for CoOOH-coupled $BiVO_4$ [101], $Co(OH)_x$-coupled Bi_2WO_4 [102], FeOOH-coupled $CuWO_4$/CdS [80], and manganese phosphate (MnPO)-coupled WO_3/$CuWO_4$ [103] photoanodes.

In addition, the PEC activity of ternary metal oxide photoelectrodes can also be enhanced by coupling with proper transition metal-based molecular catalysts. In the study by Creissen *et al.* [104], tetraphosphonated Ni bis(diphosphine) (NiP) was evaluated as a molecular catalyst to improve the PEC water reduction of $CuCrO_2$ photocathodes. Combined with the sensitization of an organic dye (DPP-P), the $CuCrO_2$|DPP-P/NiP photoelectrode showed higher photovoltage than other current state-of-the-art materials such as p-Si and GaP, making it well suited for coupling with a photoanode in tandem water splitting.

The construction of proper semiconductor/semiconductor heterojunction is another successful strategy to enhance the PEC activity of ternary metal oxide photoelectrodes. A typical example is the $BiVO_4$/WO_3 heterojunction, which significantly enhances the PEC activity of $BiVO_4$ and WO_3 [105–107]. Lee et al. investigated the effect of $BiVO_4$/WO_3, $BiVO_4$/TiO_2, $BiVO_4$/SnO_2, and $BiVO_4$/Fe_2O_3 heterojunctions on the PEC water splitting activity of $BiVO_4$ photoanode [108]. The band configurations of the above heterojunctions are presented in Fig. 6**a**. Since the valence band potential of WO_3 is more positive than that of $BiVO_4$, the holes are favorable for travel from WO_3 to $BiVO_4$. Similarly, the potential difference in the conduction band between WO_3 and $BiVO_4$ is beneficial to the separation of electrons from $BiVO_4$ to WO_3. Among these heterojunction photoanodes, $BiVO_4$/WO_3 photoanodes displayed optimum water oxidation activity. In comparison with bare $BiVO_4$ and WO_3, the optimized $BiVO_4$/WO_3 heterojunction film exhibited significant photocurrent enhancement for water oxidation (Fig. 6**b** and **6c**). Similar ternary metal oxide/photocatalyst photoelectrodes, including $BiVO_4$/BiOCl [109], Fe_2O_3/$BiVO_4$ [110], $BiVO_4$/TiO_2 [111], $BiVO_4$/$CuWO_4$ [112], $CaFe_2O_4$/$BiVO_4$ [113], MoO_3/$BiVO_4$ [114], Bi_2MoO_6/MoO_3 [115], Bi_2MoO_6/TiO_2 [116], ZnO/$ZnFe_2O_4$ [117], WO_3/$CuWO_4$ [118], BiOCl/Bi_2WO_6 [119], g-C_3N_4/Bi_2WO_6 [120], and $ZnFe_2O_4$/TiO_2 [121], have been widely investigated and exhibit improved surface charge separation and transfer efficiency for PEC water splitting. Importantly, another advantage of the construction of proper photocatalyst/ternary metal oxide heterojunction photoelectrodes is the enlargement of light absorption range. For example, the visible light absorption of Bi_2S_3/$BiVO_4$ heterojunction photoelectrodes can be extended up to 800 nm due to the presence of Bi_2S_3 [122]. Homojunction ternary metal oxide photoelectrodes (such as Bi_2MoO_6@$Bi_2Mo_2O_9$ [123] and $BiVO_4$/$Bi_4V_2O_{11}$ [29]) have also been found to have improved PEC activity relative to the bare photoelectrode due to their band matching effect.

For co-catalyst or photocatalyst-coupled ternary metal oxide photoelectrodes, the heterojunction is essentially formed between the ternary metal oxide and the coupled component regardless of the presence of photocatalysts or water splitting catalysts. In fact, many studies have investigated the ternary metal oxide-based heterojunction photoelectrodes for their synergistic effects on the charge separation and transfer as well as the promotion of PEC reaction kinetics. In the work of Gong's group. [124], p-type Co_3O_4 was introduced as an oxygen evolution catalyst to simultaneously improve the charge separation and surface reaction kinetics of $BiVO_4$ photoanode. Due to the formation of p-n heterojunction between Co_3O_4 and $BiVO_4$, the charge separation and transfer of the $BiVO_4$ photoanode was improved through the internal electric field. Meanwhile, Co_3O_4 acted as an oxygen evolution co-catalyst to improve the water oxidation reaction kinetics of $BiVO_4$ photoanode. Relative to the bare ternary metal oxide photoelectrodes, simultaneous improvement in charge separation and injection efficiency could be achieved with this type of ternary metal oxide-based heterojunction photoelectrodes. A similar enhancement in PEC performance was observed with NiO/$BiVO_4$ [125], $CuWO_4$/Mn_3O_4 [126], CoAl-LDH/$BiVO_4$ [127], and $BiVO_4$/$CoMoO_4$ [128] photoelectrodes. Based on previous reports and the above analyses, coupling of a ternary metal oxide photoelectrode with a co-catalyst with good charge transfer and separation capability is expected to improve its PEC performance.

Crystal facet-engineering

The PEC reaction is typical liquid-solid interface reaction; the active crystal facet of semiconductor photoelectrodes is the main

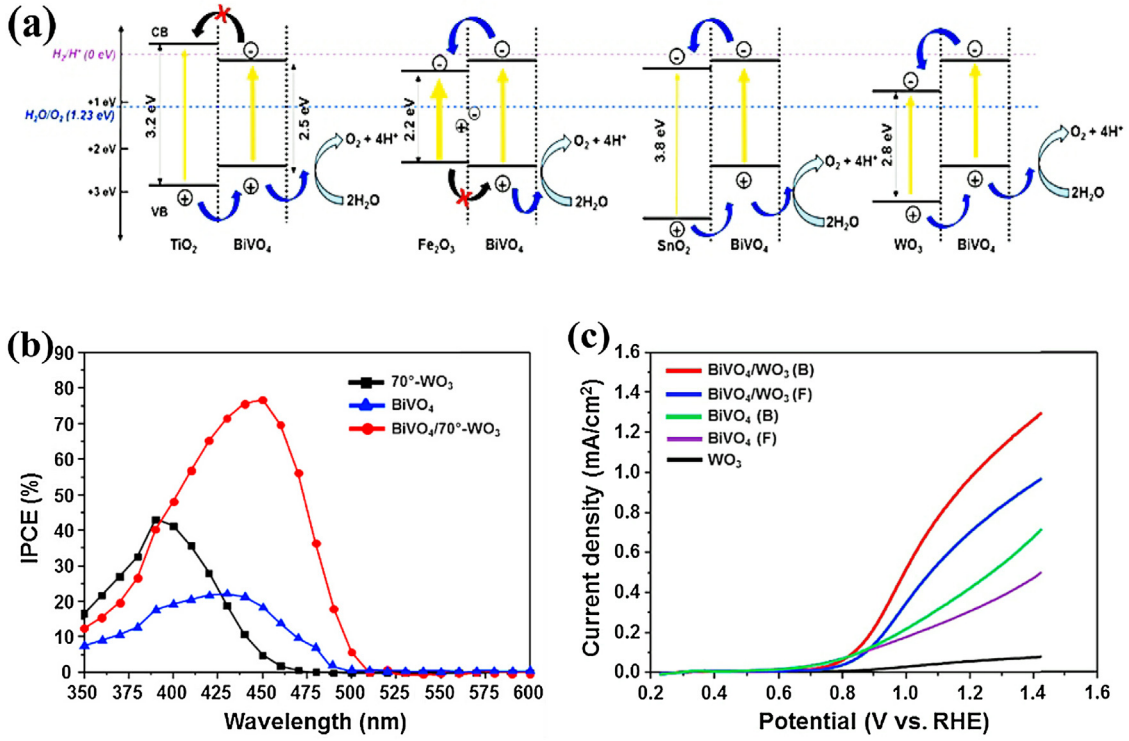

Fig. 6. (a) Schematics of the band structures of $BiVO_4$-based heterojunction; (b) IPCE spectra of $BiVO_4$, WO_3 nanorods and optimized $BiVO_4/WO_3$ nanorods; (c) Linear sweep voltammograms of $BiVO_4/WO_3$ heterojunction film; All characterizations were performed in 0.5 M phosphate buffer with 1 M Na_2SO_3 at pH 7.2. Reprinted by permission from *Ref.* [108], Copyright of 2016, Elsevier *Ltd.*.

site where the reactants react with the photogenerated charge. Consequently, the reactivity and selectivity of semiconductor photoelectrodes in heterogeneous PEC reaction is affected by their electronic and surface atomic structure, which depends on the orientation and configuration of the semiconductor crystal facet [129–131]. Specifically, the adsorption state and quantity of the reactants on the surface of photoelectrodes are intrinsically controlled by the surface atomic coordination and configuration of the semiconductor crystal facet [132]. Meanwhile, the effective mass of the charge carrier on differently orientated crystal facets are clearly different; charge carrier with smaller effective mass have higher mobility [133]. Accordingly, the charge transfer behavior and reaction kinetics of semiconductor photoelectrodes are closely related to their crystal facets. Crystal facet engineering has shown huge potential for optimizing the PEC reactivity and selectivity of ternary metal oxide photoelectrodes [134,135].

Li's group conducted a theoretical investigation of the electron and hole transport properties for all low-index $BiVO_4$ crystals by means of DFT computation [136]. The activation energy of the electron and hole transfer in low-index crystal orientations of $BiVO_4$ were calculated and denoted as $\triangle G_e$ and $\triangle G_h$, respectively (see Table 1). Among the low-index crystal facets of $BiVO_4$, the (001) facet had the lowest energy barrier of 0.194 eV for electron transfer, and the (100) facet had the lowest energy barrier of 0.433 eV for hole transfer. According to Einstein's formula, they further calculated the electron and hole mobility along the low-index crystal direction of $BiVO_4$. The mobility of the electron (μ_e) along the [010] direction of $BiVO_4$ was largest (8.53×10^{-4} cm^2/Vs) relative to the other low-index crystal directions, while the mobility of the hole (μ_h) along the [100] direction of $BiVO_4$ was largest (5.64×10^{-8} cm^2/Vs). These calculations indicate that the intrinsic electron and hole transport properties in anisotropic semiconductors are essentially related to charge separation between the different facets. Similar conclusions have been reached in previous studies that have calculated the charge transport parameters of crystal facets of $BiVO_4$ [137,138]. The as-obtained calculation results suggested that $BiVO_4$ with highly exposed (010), (001), and (100) facets may be of high photocatalytic activity.

Table 1
Electron and hole transfer paths and the corresponding facets. Reprinted by permission from *Ref.* [136], Copyright of 2015, the Royal Society of Chemistry.

Crystal Axis	Crystal Surface	ΔG_e (eV)	ΔG_h (eV)	μ_e (cm^2/Vs)	μ_h (cm^2/Vs)
[010]	(010)	0.226	0.848	8.53×10^{-4}	3.10×10^{-14}
[110]	(110)	0.576	0.707	1.36×10^{-9}	8.63×10^{-12}
[100]	(100)	0.301	0.433	9.26×10^{-6}	5.64×10^{-8}
[001]	(001)	0.194	0.734	5.56×10^{-4}	4.81×10^{-13}
[101]	(101)	0.345	0.799	3.29×10^{-6}	7.90×10^{-14}
[011]	(011)	0.231	0.844	8.36×10^{-4}	4.30×10^{-14}
[111]	(111)	0.549	0.831	1.12×10^{-9}	2.07×10^{-14}

ΔG_e and ΔG_h are the activation energy of electrons and holes, respectively; μ_e and μ_h are the mobility of electrons and holes, respectively.

In particular, Yang et al. used DFT calculations to systematically investigate the solar water oxidation reaction on $BiVO_4$ with different crystal facets; five aspects were evaluated: (1) photoexcitation, (2) electron-hole transport, (3) dipole moment, (4) water adsorption, and (5) the potential surface of O_2 evolution [138]. Their results confirmed that the water oxidation on the (010) facet of $BiVO_4$ is more favorable relative to on other low-index facets; the (010) facet is not only conducive to charge mobility, but also exhibits greater water adsorption and a lower energy barrier in the water splitting process. The charge-transport differences in different crystal facets of other ternary metal oxides have also been found in recent years [139,140]. Hashim et al. found that the surface atomic configuration of the tetragonal $PbMoO_4$ (001) facet is similar to the monoclinic $BiVO_4$ (010) facet, with the $PbMoO_4$ with (001) facet displaying high photocatalytic activity [140].

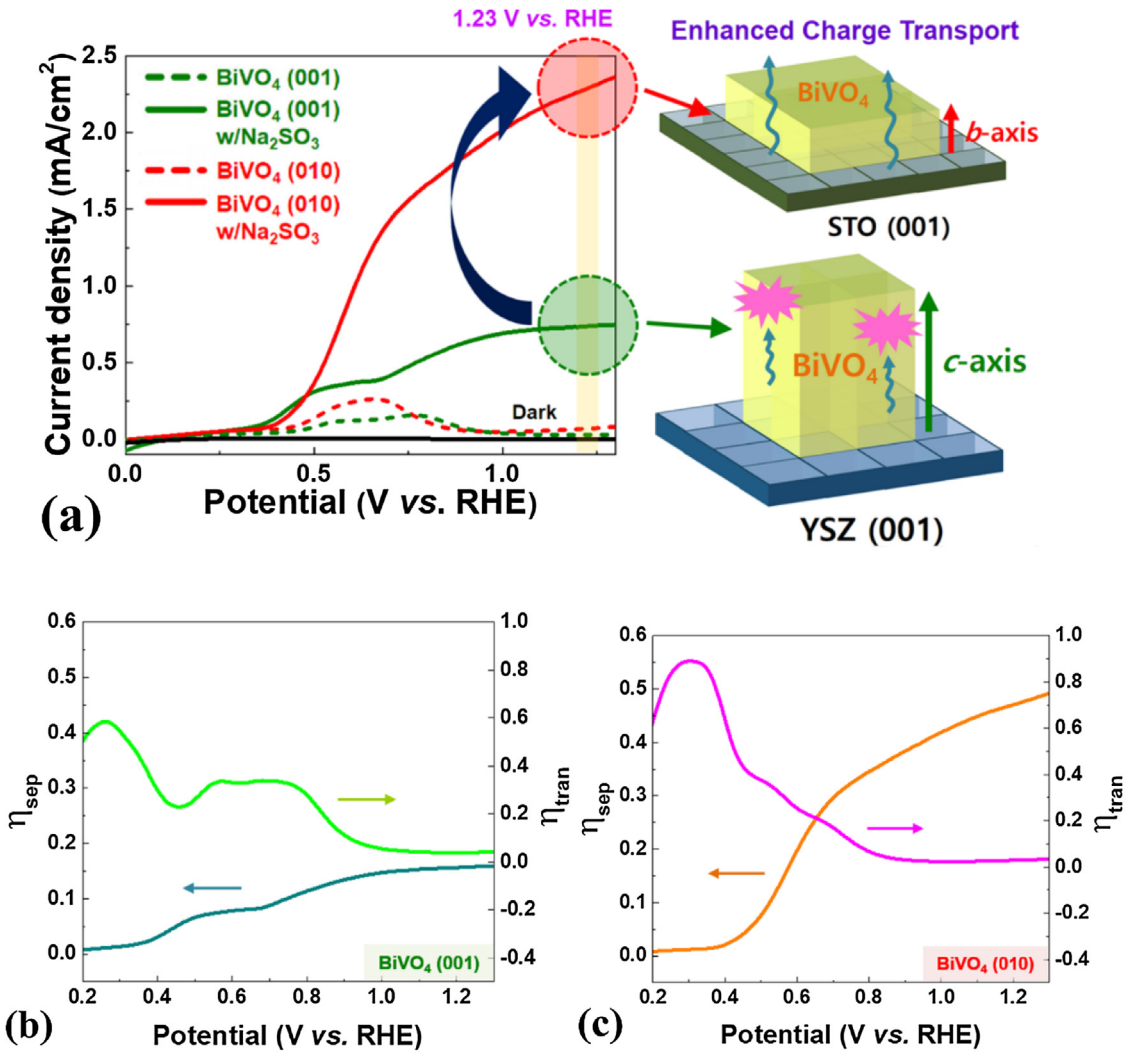

Fig. 7. (a) Schematic of epitaxial $BiVO_4$ thin films grown in the *c*-axis orientation on a YSZ (001) substrate and in the *b*-axis orientation on an STO (001) substrate and corresponding linear sweep voltammetry curve in 0.5 M Na_2SO_4 aqueous solutions in the presence or absence of 0.5 M Na_2SO_3 as the hole scavenger. Charge separation efficiencies (η_{sep}) and surface transfer efficiencies (η_{tran}) of 100 nm-thick epitaxial (b) $BiVO_4$ (001) and (c) $BiVO_4$ (010) thin films. Reprinted by permission from *Ref.* [141], Copyright of 2018, the American Chemical Society.

In the experimental study of Song et al., epitaxial $BiVO_4$ film with different crystallographic orientations was synthesized and investigated as a photoanode for water oxidation [141]. The *c*-axis-oriented epitaxial $BiVO_4$ (001) film was grown on yttria-stabilized zirconia (001) substrates, whereas the *b*-axis-oriented epitaxial $BiVO_4$ (010) film was grown on $SrTiO_3$ (001) substrates (shown in Fig. 7). The photocurrent density of $BiVO_4$ with a (010) orientation (2.29 mA cm^{-2}) was much higher than that of $BiVO_4$ with a (001) orientation (0.74 mA cm^{-2}) in 0.5 M Na_2SO_4-Na_2SO_3 at 1.23 V *vs.* RHE. Further, the $BiVO_4$ film with a (010) orientation exhibited a marked improvement in PEC water oxidation activity relative to the $BiVO_4$ film with a (001) orientation. The PEC activity difference on the two orientations of $BiVO_4$ film can primarily be attributed to the charge transport property differences between the (010) and (001) orientations. The specific influence of crystal facets on the PEC activity of $BiVO_4$ requires further study and identification. Recent work by Han et al. reported differing PEC activity observations on a $BiVO_4$ photoanode with a preferred [001] orientation [142]. They observed that pristine $BiVO_4$ with a preferred [001] growth orientation and exposed (001) facet has excellent PEC water oxidation activity. In addition, our recent study indicated that the $BiVO_4$ polyhedral films with exposed {121}, {132}, {211}, and {251} high-index facets have higher activity and faster PEC water oxidation kinetics than the normal $BiVO_4$ films with only {121} mono-high-index facet [143]. The adsorption of H_2O molecules on $BiVO_4$ {121} and {132} high-index facets is energetically favorable for subsequent dissociation and oxidation relative to that on {010} and {110} low-index facets. Furthermore, the water oxidation limiting step and its overpotential on the {121} and {132} high-index facets of $BiVO_4$ is different from that on the {010} and {110} low-index facets (shown in Fig. 8) [143]. On the basis of the above data, we presumed that the high-index crystal facets of $BiVO_4$ could provide highly active catalytic sites to decrease the overpotential for the PEC reaction, thereby improving the PEC kinetics of $BiVO_4$ photoelectrodes. On the other hand, the low-index facets of $BiVO_4$ potentially affect the charge separation and transfer property; thus, enhanced PEC activity can be achieved on $BiVO_4$ photoelectrodes with proper low-index facets.

Crystal facet engineering also functions to regulate the surface energy of semiconductor photoelectrodes. The structure of ternary metal oxide photoelectrodes comprises multi-atom orbital hybridization, which usually results in the formation of dangling bonds and high surface energy. Ternary metal oxide photoelectrodes with high energy surface states generally form native

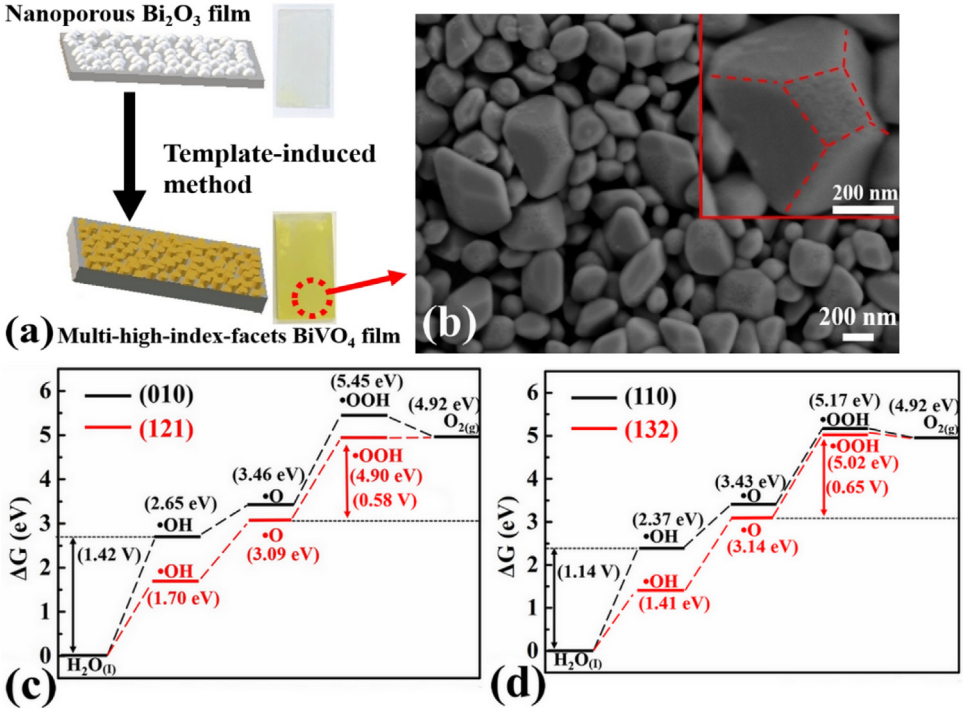

Fig. 8. (a) Schematic illustration of the preparation procedure and (b) typical SEM image of $BiVO_4$ film with multi-high-index facets. Free-energy diagrams for the four steps of the PEC water oxidation on the (c) (010), (121) and (d) (110), (132) facets of BiVO4 at U = 0, pH = 6.8, and T = 298 K. The ΔG (vertical sold line with arrows) value of the rate-determining step is shown for each surface. Reprinted by permission from *Ref.* [143], Copyright of 2018, the American Chemical Society.

electron-hole recombination centers on their surface; these are disadvantageous for the PEC reaction. For example, the broken Bi-O dangling bonds on the crystal facets of $BiVO_4$ induce its high surface energy [144,145], which leads to high recombination of surface charge. Kim et al. calculated and compared the surface energy of typical crystal facets of $BiVO_4$ [146]. They found that the $BiVO_4$ (001) facet has the highest surface energy of 2.5234 J/m^2, while the (040) facet has the lowest surface energy (0.0479 J/m^2). Based on these calculations, Kim et al. synthesized a (040)-crystal facet engineered $BiVO_4$ photoanode for water oxidation. Due to the lower surface energy, the $BiVO_4$ photoanode with a (040) facet was favorable for charge carrier mobility, and thus higher solar light energy conversion efficiency was achieved. Their findings may be used to explain the previous experimental observation of enhanced PEC performance on the $BiVO_4$ photoanode with exposed (040) facets [147].

Since the electronic density states and structures of crystal facets determine the band position of semiconductor, in addition to the regulation of reactivity, the selectivity of ternary metal oxide photoelectrodes can also be altered through crystal facet engineering [148]. For instance, Song et al. reported that the $BiVO_4$ (010) film has a narrower band gap of *ca.* 2.68 eV relative to the $BiVO_4$ (001) film (*ca.* 2.72 eV) [141]. Hu et al. found that the surface energy level of the minimum conduction band was more positive for $BiTaO_4$ predominantly surrounding the (001) facet than that for typical $BiTaO_4$ [149]. Thus, the (001) facet of $BiTaO_4$ with a higher conduction band can generate more reductive electrons, which is beneficial for the photocatalytic reaction.

At present, crystal facet engineering of ternary metal oxides has primarily been performed on powder-photocatalysts [150–152]. The development of crystal facet engineering on ternary metal oxide photoelectrodes is a challenge due to the difficult preparation of ternary metal oxide films with the desired facets. Therefore, efforts are needed to overcome the preparation bottleneck of ternary metal oxide films and to clarify the PEC reaction mechanisms on different crystal facets of ternary metal oxide photoelectrodes.

Photoelectrochemical applications of ternary metal oxide photoelectrodes

Photoelectrochemical water splitting

Ternary metal oxide photoanodes

Metal vanadates. $BiVO_4$ is typical metal vanadate, and has been identified to be one of the most promising photoanode materials due to its unique band structures and properties [153]. A moderate band gap of ~2.4 eV allows it to absorb ~11% solar light and achieve a theoretical maximum AM1.5 G photocurrent of ~7.6 mA cm^{-2}, reflecting a STH efficiency of ~9.3%. Well-positioned band edges (conduction band minimum at ~0 V vs RHE) enable it to generate considerable photocurrent at a relatively low bias as compared to the onset of dark water oxidation (1.23 V vs RHE). $BiVO_4$ was first investigated as a photoelectrode around 1999 [154], and since then this vanadate has received extensive research attention with respect to solar water splitting. However, initially, $BiVO_4$ did not exhibit PEC water oxidation performance (only a few tenths of mA cm^{-2} in photocurrent) as expected due to several limitations including poor charge transport properties and sluggish water oxidation kinetics. Previous research has found that charge carrier of $BiVO_4$ are transported via a small polaron hopping conduction mechanism which results in relatively low carrier mobility [24,30]. As described in the above sections, numerous attempts have been made to address these performance issues for $BiVO_4$ photoanode. Among them, $WO_3/BiVO_4$+CoP_i core-shell nanostructured photoanodes exhibit an impressive water oxidation photocurrent of 6.72 mA cm^{-2} under AM 1.5 G illumination at 1.23 vs RHE, which corresponds to ~90% of the theoretically possible value for $BiVO_4$ [155]. Fig. 9 illustrates the micro-structure and functional mechanisms of $WO_3/BiVO_4$+CoP_i photoelectrode for solar water splitting.

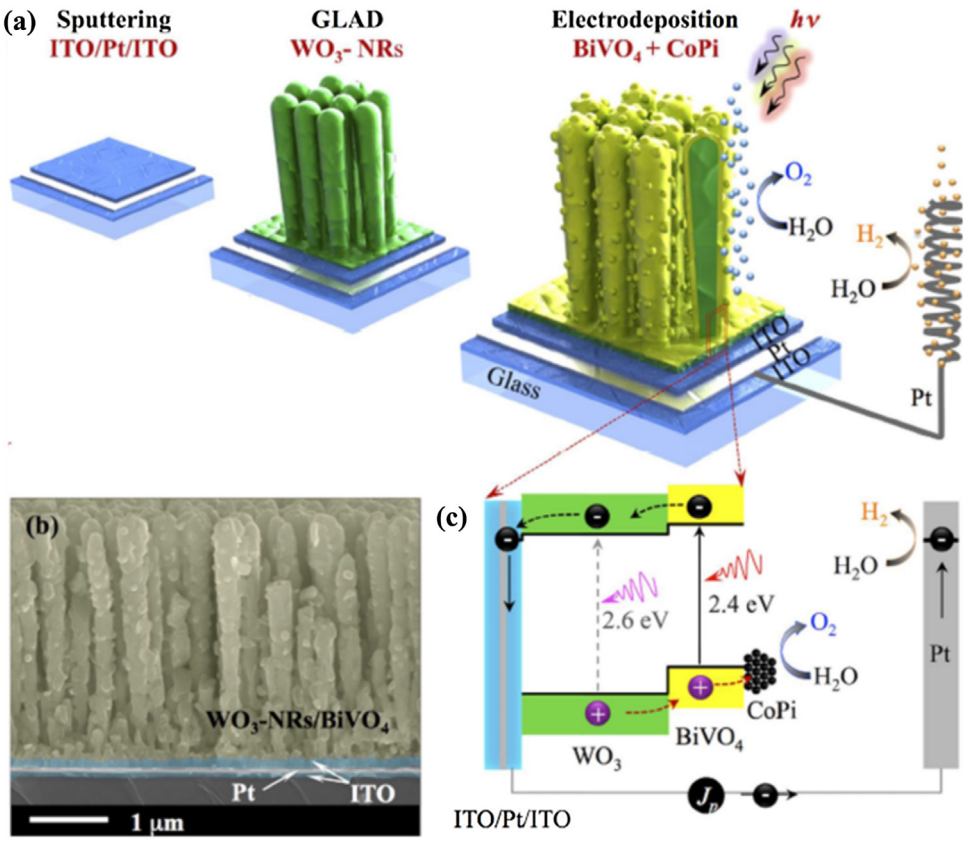

Fig. 9. (a) Schematic illustration of a core-shell WO_3-NRs/$BiVO_4$ photoanode fabricated by glancing angle deposition (GLAD) of WO_3-NRs followed by electrodeposition of $BiVO_4$+CoP_i. (b) The SEM image shows a cross section of the ITO/Pt/ITO/WO_3-NRs/$BiVO_4$ + CoP_i photoanode. (c) Schematic illustration of a PEC water splitting cell with the ITO/Pt/ITO/WO_3-NRs/$BiVO_4$ + CoP_i photoanode and Pt cathode. Reprinted by permission from *Ref.* [155]. Copyright of 2015, Nature Publishing Group.

Notably, the maximum STH efficiency of $BiVO_4$ photoelectrode with a light adsorption edge of ~516 nm is only ~9.3%, which is below the threshold for the practical application of PEC water splitting (10%). Hence, the exploration of other metal vanadates with narrow band gap has been simultaneously conducted in recent years. Copper(II)-based vanadates (such as, α-CuV_2O_6, α-$Cu_2V_2O_7$, β-$Cu_2V_2O_7$, γ-$Cu_3V_2O_8$, and $Cu_{11}V_6O_{26}$) with band gap at or below 2 eV have been investigated as potential photoanodes due to their superior visible light absorption ability [156–160]. Zhou et al. explored four copper-based vanadates are composed of divalent copper and pentavalent vanadium (α-$Cu_2V_2O_7$, β-$Cu_2V_2O_7$, γ-$Cu_3V_2O_8$, and $Cu_{11}V_6O_{26}$) as photoanodes using high throughput combinatorial discovery techniques [156]. They found that the Fingerite phase ($Cu_{11}V_6O_{26}$) exhibits excellent stability in a strong alkaline electrolyte, while McBirneyite phase (γ-$Cu_3V_2O_8$) has admirable PEC activity (1.5 mA cm^{-2} in pH 9 electrolyte) and photostability in electrolytes with pHs of 7, 9, and 13. Seabold et al. prepared porous $Cu_3V_2O_8$ thin films using the dip-coating method and investigated its physical properties and PEC activity [157]. They investigations indicated that $Cu_3V_2O_8$ possesses an indirect band gap of 2.05 eV and its flat-band potential is around 0.66 V vs RHE. Meanwhile, the electron diffusion length and O_2 evolution faradaic efficiency of $Cu_3V_2O_8$ photoanode were ~100 nm and near 100%, respectively, within three minutes of measurement. In previous work, we have prepared and investigated CuV_2O_6 and $Cu_2V_2O_7$ thin films as photoanodes for solar water splitting [158]. The photocurrent density of CuV_2O_6 and $Cu_2V_2O_7$ films at 1.23 V vs RHE in 0.1 M NaB_i buffer solution were about 25 and 35 μA/cm^2, respectively. Lumley and co-workers reported an n-type $Cu_{11}V_6O_{26}$ with a bad gap of 1.9 eV, and the $Cu_{11}V_6O_{26}$ showed PEC water splitting activity in weak alkaline solution [160]. In addition, Zhou et al. investigated the stability of several copper vanadates through combination of Pourbaix calculations and combinatorial experimentation. Their study revealed that the Cu-rich vanadates ($Cu_{11}V_6O_{26}$ and γ-$Cu_3V_2O_8$) can attain long-term PEC stability by self-passivation [159]. It is worth noting that, with increasing Cu:V atomic ratio, the Cu-rich vanadates exhibited higher absorption coefficients and charge separation efficiency, but lower charge injection efficiency due to the charge recombination at Cu-related surface states. Given its physical properties and PEC activity, γ-$Cu_3V_2O_8$ is considered to be the most promising copper vanadate photoanode for solar water splitting. An illustration of the band structure of γ-$Cu_3V_2O_8$ is shown in Fig. 10**a**. Nevertheless, as shown in Fig. 10b, previous efforts have not yet yielded a suitable photocurrent density (dozens of μA cm^2) despite the relatively narrow band gap of γ-$Cu_3V_2O_8$ (maximum theoretical photocurrent density is ~13 mA cm^2). The unsatisfactory PEC activity of γ-$Cu_3V_2O_8$ is probably attributed to its short hole diffusion length (20–40 nm) and large absorption depth, as reported by Jiang et al. (Fig. 10**c** and **d**) [161]. Therefore, future researches should focus on these disadvantages to expand the utilization potential of copper vanadate photoanodes.

In addition to the copper-based vanadates, several other metal-based vanadates also have been investigated as photoanode materials for PEC water splitting. Yan et al. identified β-$Mn_2V_2O_7$ as a highly promising light absorber with a desirable band gap of ~1.75(± 0.1) eV for PEC water splitting [162]. Although β-$Mn_2V_2O_7$ is not very photoactive for water oxidation, its position of conduction and valence band match very well for water redox potentials. $FeVO_4$ was synthesized and investigated as a photoanode material for solar water oxidation by Morton's group [163]. Their findings revealed that $FeVO_4$ has an indirect band gap of ~2.0 eV and its

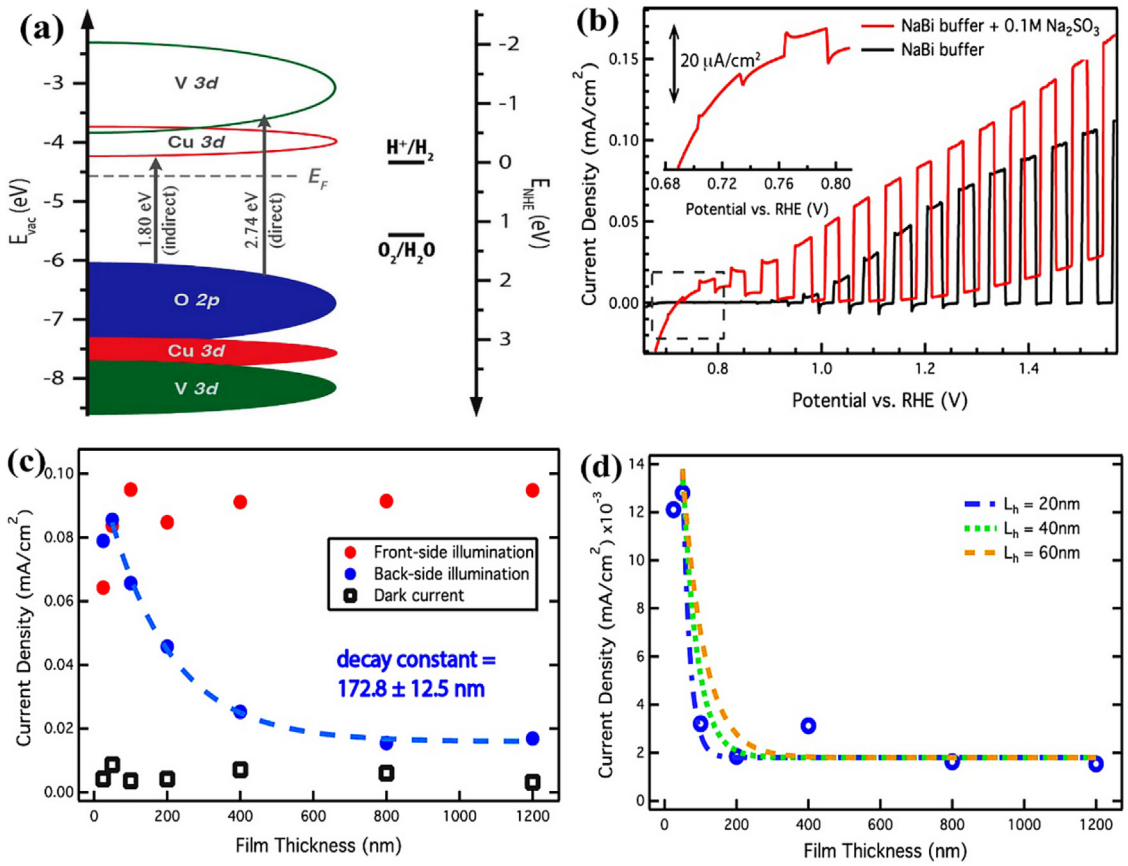

Fig. 10. (a) Illustration of the optoelectronic structure of γ-$Cu_3V_2O_8$ with respect to the vacuum level. (b) Linear sweep voltammetry (LSV) measurement of a γ-$Cu_3V_2O_8$ photoelectrode under chopped front-side illumination by simulated AM1.5 irradiation at 1 sun intensity. The scan rate was 50 mV/s. (c) Photocurrent densities under AM1.5 G simulated irradiation at 1 sun intensity, with illumination from the front-side (red) and back-side (blue), as a function of film thickness. (d) Backside illuminated photocurrent density with 340 nm irradiation. Dashed lines are the modeled photocurrent decay with 20, 40, and 60 nm hole diffusion lengths. All measurements were obtained at an applied electrochemical bias of 1.23 V versus RHE. Reprinted by permission from *Ref.* [161], Copyright of 2017, the American Chemical Society.

photocurrent gradually increase with increasing annealing temperature. Mandal et al. studied three different stoichiometric iron vanadates ($FeVO_4$, FeV_2O_4, and Fe_2VO_4), and found FeV_2O_4 has the highest photocurrent (0.18 mA cm^{-2} at 1.0 V vs Ag/AgCl) under 100 mW cm^{-2} illumination [164]. NiV_2O_6, another a metal-based vanadate capable of absorbing visible light, has been demonstrated to have a direct band gap of 2.38 eV and shows measurable photoactivity under visible light illumination [84]. Sameie et al. investigated the structural, electronic, and optical properties of two photoanode candidates, ZnV_2O_6 and $Zn_2V_2O_7$, using first principles calculations [165]. Their results showed that ZnV_2O_6 and $Zn_2V_2O_7$ have favorable band gaps (2.31 and 2.52 eV) and appropriate band edge positions for the oxygen evolution reaction. $InVO_4$, with an indirect band gap of 3.2 eV, was reported to have a flat band potential of -0.04 V *vs.* RHE and high stability over a wide pH range (3–11) [166]. Chemelewski and co-workers systematically studied the PEC properties of α-Ag_3VO_4 thin films [167]. Although most studies have suggested that the PEC activity of above metal-based vanadates for solar water splitting is not satisfactory, these works revealed many intrinsic properties of metal-based vanadates and provided reference to develop more efficient ternary metal oxide photoelectrodes in future.

Metal tungstates and molybdates. Among the ternary metal tungstates, triclinic $CuWO_4$ has been extensively studied as photoanode material due to its small band gap (~2.3 eV) capable of using visible light, high Faradaic oxygen evolution efficiency in a variety of electrolytes, and robust stability under highly oxidizing conditions [168]. As shown in Fig. 11a, $CuWO_4$ has a triclinic crystal structure (space group $P\bar{1}$), where the metal–oxygen Jahn–Teller distorted octahedral (CuO_6 and WO_6) of one type shares edges and forms zigzag chains along the c-axis. The zigzag chains are arranged in alternating layers that are perpendicular to the a-axis direction [169]. In comparison with WO_3, the narrower band gap of $CuWO_4$ can be explained by the lower valence band edge due to the hybridization of Cu(3d) and O(2p) orbitals (Fig. 11**b**) [168]. The improved stability of $CuWO_4$ in a neutral electrolyte compared to WO_3 can also be traced to the strong Cu-O bond, which limits the formation of soluble tungstate. Due to the potential PEC activity of $CuWO_4$, various methods have been applied to synthesize $CuWO_4$ films for PEC water oxidation. Significantly, the pristine $CuWO_4$ photoanode does not exhibit expected activity for solar water oxidation. Bartlett's group systematically investigated the mechanisms of charge transport in $CuWO_4$, and attributed the mismatching performance of $CuWO_4$ photoanode for solar water oxidation to the sluggish hole transfer from the photoanode to the electrolyte [170]. From their electrochemical impedance spectroscopy measurements, a midgap state is identified in $CuWO_4$, as illustrated in Fig. 11**c**. The midgap state of $CuWO_4$ is likely composed of Cu(3d) orbitals, which could act as recombination centers for the holes and electrons on the surface of $CuWO_4$ photoanode, and affect the transfer of charge at the interface between the photoanode and electrolyte. In their work, this mid-gap state has been considered to be a permanent state in the electronic structure of $CuWO_4$, rather than a photogenerated one. However, a recent study by Gao et al. suggested that the surface impediment of $CuWO_4$

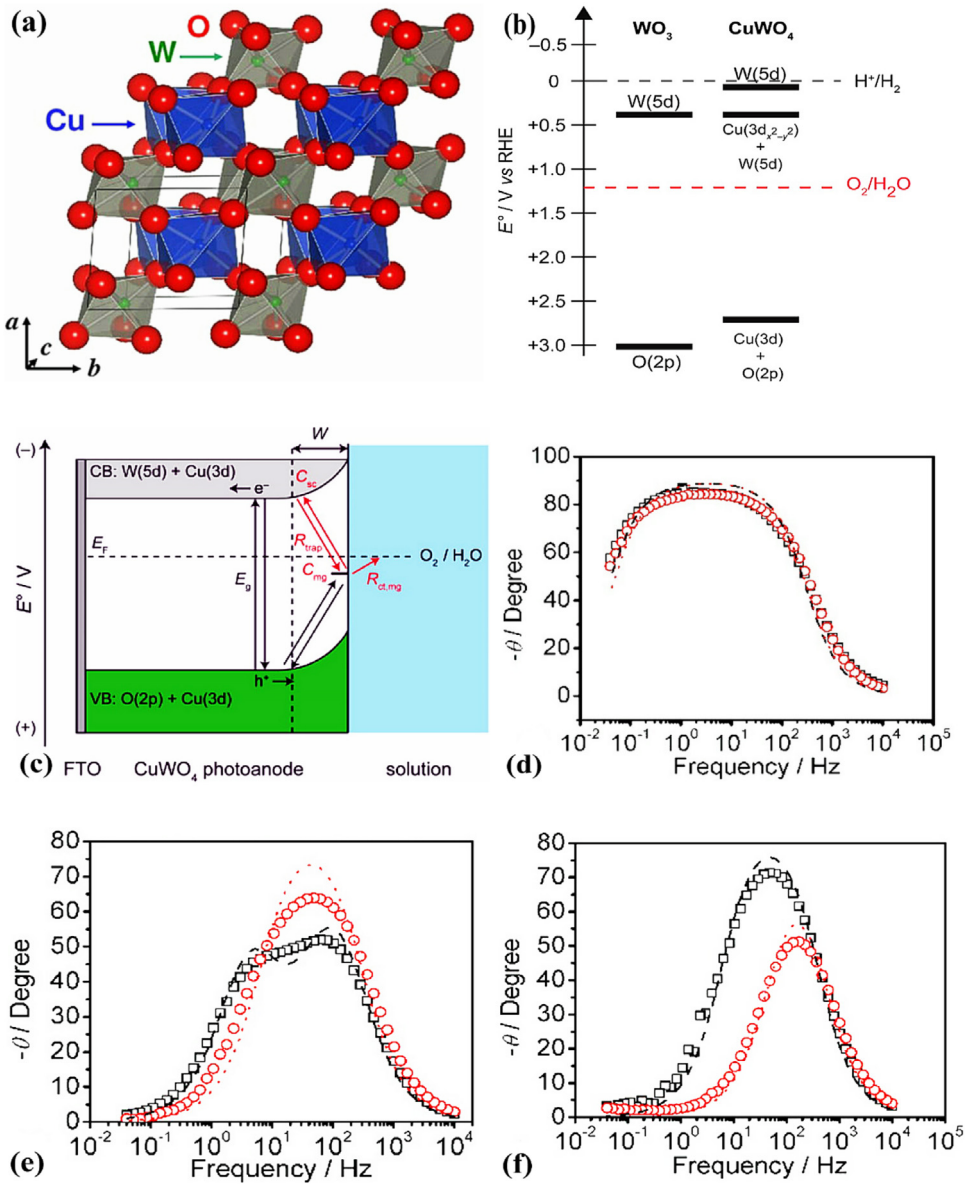

Fig. 11. (a) Crystal structure and the first Brillouin zone of the triclinic $CuWO_4$ (space group *P1* (No. 2)). Reprinted by permission from *Ref.* [169], Copyright of 2012, Elsevier *Ltd.*. (b) Electronic structures of $CuWO_4$ and WO_3. Band edge potentials are referenced to the reversible hydrogen electrode, RHE. Reprinted by permission from *Ref.* [168], Copyright of 2016, the American Chemical Society. (c) Proposed physical model for charge-carrier pathways in $CuWO_4$: excitation, midgap state trapping, and charge-transfer reactions to solution. *W* represents the depletion width, and the red arrows correspond to the charge-transfer processes measured by EIS. Reprinted by permission from *Ref.* [170], Copyright of 2013, the American Chemical Society. Bode phase plots of $CuWO_4$ electrode at 0.93 V vs RHE (d) in the dark and (e) under 1 sun illumination and (f) at 1.53 V vs RHE under 1 sun illumination. Data measured in H_2O (black squares) and 0.5 M Na_2SO_3 (red circles) are shown. Fitted curves are shown as black dashed lines for H_2O and red dotted lines for Na_2SO_3. Reprinted by permission from *Ref.* [171], Copyright of 2017, the American Chemical Society.

photoanode is due to the buildup of water oxidation intermediate species on the surface of $CuWO_4$, rather than a permanent or intrinsic midgap as reported by Pyper et al. [171]. The authors constructed Bode plots indicating the capacitive elements that appear in the electrochemical impedance spectroscopy (Fig. 11d, e, and f). In the dark, the plots only showed one peak at all potentials in either a H_2O or Na_2SO_3 electrolyte. Under illumination, two capacitive peaks were clearly observed in the Bode phase plot for $CuWO_4$ electrodes in the H_2O electrolyte. Further, there was only one peak observed under illumination in the Na_2SO_3 electrolyte. Therefore, the authors assigned this peak to a water oxidation intermediate species as opposed to an intrinsic state. These efforts provided insight into the PEC activity limitation of $CuWO_4$ photoanode, and suggested the development directions with regard to potential modification strategies to further improve its PEC activity.

Furthermore, Bi_2WO_6 and Bi_2MoO_6 have been studied as potential W or Mo-based ternary oxide photoanodes for solar water oxidation. The band gap of Bi_2WO_6 was reported to be 2.7–2.8 eV, and its conduction band edge was slightly more negative than the potential of proton reduction, meeting the thermodynamic requirements for PEC water splitting with low or no applied bias. Hill et al. prepared polycrystalline Bi_2WO_6 photelectrodes using a combination approach of electrochemical deposition and thermal treatment, and investigated their photocurrent-to-O_2 conversion efficiency and photostability [172]. Although Bi_2WO_6 suffers from photocorrosion, improving its charge transport property could make Bi_2WO_6 a promising photoanode for solar water oxidation. Bi_2MoO_6 also be investigated as photoanode material owing to its appropriate band gap (2.5–2.8 eV), excellent chemical stability, and photocorrosion resistance. Cai et al. synthesized a novel

3D Bi_2MoO_6-based photoelectrode and achieved a suitable photocurrent for solar water oxidation by applying self-supported Si nanowires as core materials [173]. Additionally, α-$SnWO_4$ [174], Fe_2WO_6 [175], $NiWO_4$ [176], $ZnWO_4$ [177], $CdWO_4$ [178], $Bi_2Mo_2O_9$ [123], and $Bi_2Mo_3O_{12}$ [179] have also been identified as photoanodes for solar water oxidation. The physical properties and PEC activity of these photoanode materials are summarized in Table 2.

Other ternary metal oxides. In the past years, several spinel ferrites (MFe_2O_4, M = Zn, Cu, Mg, Ca) have been investigated as photoanode materials for solar water oxidation. Typically, n-type $ZnFe_2O_4$ has attracted significant attention owing to its small band gap of ~2.0 eV, its photochemical stability in basic electrolyte, and its suitable valance band position [180]. Since the water oxidation activity of pristine $ZnFe_2O_4$ photoanode fall short of expectations, $ZnFe_2O_4$ usually be applied as a component to couple with other photocatalysts, and form heterojunction photoelectrodes with higher PEC activity. For example, given that the conduction band position of $ZnFe_2O_4$ is ~0.2 V more negative than that of Fe_2O_3, the α-Fe_2O_3/$ZnFe_2O_4$ heterojunction photoelectrode shows a significantly enhanced water oxidation performance compared to bare Fe_2O_3 and $ZnFe_2O_4$ photoelectrode [82]. Similar improvement in PEC activity was observed on $BiVO_4$/$ZnFe_2O_4$ [181], TiO_2/$ZnFe_2O_4$ [182] and ZnO/$ZnFe_2O_4$ photoelectrodes [183]. In more recent work, the PEC activity of $ZnFe_2O_4$ photoelectrode was improved with a hybrid microwave annealing method by improving the crystallinity and reducing the surface defect states of the material [184]. This work highlights the potential of $ZnFe_2O_4$ for solar water splitting; its performance is expected to be further improved through other modification strategies like doping or nanostructuring [76,82]. Furthermore, $SrTiO_3$ [185], $CaTiO_3$ [186], $MnTiO_3$ [187], $FeTiO_3$ [187], $CoTiO_3$ [187], $NiTiO_3$ [187], Sn_2TiO_4 [188], $CuFe_2O_4$ [189], $BiFeO_3$ [190], and $CuSnO_3$ [191] have also been synthesized and investigated as photoanodes for solar water oxidation. The physical properties and PEC activity of these ternary metal oxide photoanodes are summarized in Table 2. Among them, $SrTiO_3$ has attracted significant research attention because it can transfer from an n-type to a p-type through Rh doping [192].

Ternary metal oxide photocathodes

Copper-based ternary metal oxides are investigated as photocathode materials for solar water reduction. Among these various copper-based ternary metal oxides, $CuFeO_2$ has been most studied due to its small band gap (~1.5 eV), relatively positive onset potential, abundant resources, and relatively good photostability in aqueous electrolytes (Fig. 12**a**) [193]. Read et al. synthesized $CuFeO_2$ film using a facile electrochemical method, and demonstrated that $CuFeO_2$ film is capable of photoelectrochemically producing H_2 using the entire range of the visible spectrum [193]. Unfortunately, they also demonstrated that pristine $CuFeO_2$ is of poor PEC activity for H_2 evolution. Prévot et al. prepared thin films of p-type $CuFeO_2$ using a sol-gel-based technique [194]. The PEC activity of as-prepared $CuFeO_2$ film was enhanced by improving its charge separation and transport properties through thermally intercalating oxygen in its layered structure. More recently, Jang et al. reported a $CuFeO_2$ thin film and demonstrated that hybrid microwave annealing (HMA) can increase its photocurrent density by improving its charge transport property (Fig. 12d) [195]. Although these studies have demonstrated that $CuFeO_2$ is a promising photocathode material for solar water reduction, continued efforts focusing on increasing its charge separation efficiency and optimizing its interface are needed for further expansion of its PEC application.

P-type $CuBi_2O_4$ has also been intensively investigated as photocathode material for water reduction because of its impressive absorption ability of visible light and suitable band edge position for water reduction reaction [196–200]. As shown in Fig. 13a, the structure of $CuBi_2O_4$ consists of planar CuO_4 complexes that are stacked along the c-axis in a staggered manner. Between the stacks of CuO_4, each Bi atom is connected to six O atoms with three different bond distances [197]. Hahn et al. synthesized thin films of p-$CuBi_2O_4$ by electrodeposition and investigated their PEC activity for solar water reduction [197]. Similar as most of copper-based ternary metal oxides, pristine $CuBi_2O_4$ photoelectrodes exhibited a relatively low photocurrent density for water oxidation reaction. For the modification of $CuBi_2O_4$ photocathode, Berglund et al. did several classic works. They firstly found that Ag-doping can improve the PEC activity of $CuBi_2O_4$ using SECM technique [198]. Then, this observation was demonstrated by Kang et al. (Fig. 13b) [199]. In addition, Berglund et al. demonstrated that PEC performance limiting factors of $CuBi_2O_4$ photocathode and provided a gradient self-doping way to improve the charge separation efficiency of $CuBi_2O_4$ photocathode (Fig. 13c and d) [200]. In general, these efforts have significant improvement in PEC activity $CuBi_2O_4$ photocathode, but the PEC stability issue of $CuBi_2O_4$ that originated from its photo-corrosion is still challenging.

Apart from copper-based ternary metal oxides, other p-type ternary metal oxides have been widely investigated as photocathode materials for solar water splitting. Fox example, Park et al. investigated p-type $AgRhO_2$ as a photocathode material for PEC water splitting [201]. It was found that $AgRhO_2$ has a band gap of ~1.7 eV and a flat band potential of ~0.51 V vs. Ag/AgCl in 0.5 M KNO_3. The $AgRhO_2$ photocathode exhibited nearly 100% Faradaic efficiency for H_2 evolution across a wide range of pH values, as well as good photostability. Similar identification was performed on several ternary metal oxides, such as $CuFe_2O_4$ [202], $CaFe_2O_4$ [203], $NiFe_2O_4$ [204], $CuNbO_3$ [205], $CuCrO_2$ [206], $CuRhO_2$ [207], $CuYO_2$ [208], $CuGaO_2$ [209], $CuMnO_2$ [210], and $PbMoO_4$ [211]. Some of the physical properties and PEC activity of these p-type ternary metal oxides are summarized in Table 3.

Photoelectrochemical organic synthesis

PEC water splitting is a clean approach to produce H_2 fuel using solar energy, but the activity of hydrogen evolution on the cathode is usually restricted by the sluggish kinetics of the oxygen evolution on the photoanode [215,216]. H_2 fuel is actually the desired product of PEC water splitting, while the O_2 produced from the photoanode has a lower economic value. In recent years, PEC organic synthesis has been developed as an alternative to the production of O_2 on the photoanode; it is considered to be an environmentally friendly approach to produce valuable organic products using solar energy [8]. Like PEC water splitting, PEC organic synthesis is essentially driven by the photoinduced holes or electrons from the semiconductor photoelectrodes under solar illumination [217,218]. Therefore, if a suitable organic reaction is initiated by the photogenerated holes on the photoanode, H_2 fuel can be obtained on the cathode simultaneously. The combination of PEC water splitting and organic synthesis will increase the economic value of products obtained from semiconductor photoelectrodes, and the limitations of kinetically unfavorable oxygen evolution on the photoanode can potentially be addressed. As the heart of the PEC cell, the fundamental properties of photoelectrodes determine its efficiency for water splitting and organic synthesis. In this section, several PEC organic synthesis reactions on ternary metal oxide photoelectrodes are highlighted, and the selection of the solvent, photoelectrode material, and redox mediator for PEC organic synthesis are discussed.

5-hydroxymethylfurfural (HMF) is an important intermediate in biomass conversion; it can be used as a platform molecule to produce several industrial chemicals. 2, 5-furandicarboxylic acid

Table 2
Key material properties and PEC activity parameters of ternary metal oxides that have been identified as photoanodes for solar water oxidation.

Ternary metal oxide		Synthetic method	Band gap (eV)	Light source and filter	Flat-band potential	Electrolyte and pH	Photocurrent (mA/cm^2)[a]	Reference
Vanadates	$BiVO_4$	Electrodeposition	~2.5	300 W Xe lamp AM 1.5 G	~0.11 V vs. RHE	0.5 M KP_i (7)	~1.7	Ref. [100]
	α-CuV_2O_6	Drop-casting	~1.95	150 W xenon lamp AM 1.5 G	0.74 – 0.80 V vs. RHE	0.1 M NaBi (9.2)	~0.025	Ref. [158]
	α-$Cu_2V_2O_7$	Sputter deposition	1.9 ± 0.1	ABET Sun 3000 AM 1.5 G	/	KBi buffer (9.2)	1.5-2	Ref. [156]
	β-$Cu_2V_2O_7$	Drop-casting	~1.98	150 W xenon lamp AM 1.5 G	0.68 – 0.77 V vs. RHE	0.1 M NaBi (9.2)	~0.035	Ref. [158]
	γ-$Cu_3V_2O_8$	Dip-coating	2.05	300 W Xe arc lamp $GaP_{0.98}N_{0.02}$ photodiode	0.66 V vs. RHE	0.1 M KBi (9.2)	~0.018	Ref. [157]
	$Cu_{11}V_6O_{26}$	Co-sputtering	1.80	16S-300 – 002 AM 1.5 G	0.70 V vs. RHE	NaBi buffer (9.2)	~0.062	Ref. [161]
		Electrodeposition+ Thermal treatment	1.90	300 W Xe lamp AM 1.5 G	0.64 – 0.73 V vs. RHE	NaBi buffer (9.2)	~0.010	Ref. [160]
	$Cu_5V_2O_{10}$	Co-sputtering	1.83	16S-300-002 AM 1.5 G	/	0.1 M KBi (9.3)	~0.053	Ref. [212]
		Co-sputtering	2.03	16S-300-002 AM 1.5 G	/	0.1 M KBi (9.3)	~0.001	Ref. [212]
	$FeVO_4$	Precipitation+ Drop casting	2.00	150WXe lamp AM 1.5 G		0.5 M NaOH	~0.012	Ref. [163]
		Drop casting	~1.9 eV	300 W Xe arc lamp	0.08 V vs. Ag/AgCl	Phosphate buffer + 0.1 M SO_4^{2-}	~0.025	Ref. [164]
	$Fe_2V_4O_{13}$	SILAR	~2.3 eV	150 W xenon lamp AM 1.5 G	0.5 V vs. RHE	0.1 M NaBi (9.2)	~0.016	Ref. [213]
	NiV_2O_6	Co-evaporating	~2.4 eV	150 W xenon lamp AM 1.5 G	0.6 V vs. RHE	1 M KOH	~0.020	Ref. [84]
	$InVO_4$	Spray pyrolysis	~3.2 eV	375 nm LED	−0.04 V vs. RHE	0.1 M KOH	~0.0001	Ref. [166]
	Ag_3VO_4	SILAR	2.2 eV	150 W Xe lamp AM 1.5 G	/	0.2 M Na_2CO_3	~0.0018	Ref. [167]
	$CuWO_4$	Electrodeposition	2.25 eV	150 W Xe lamp AM 1.5 G	+0.4 V vs. RHE	0.1 M KP_i (7.0)	~0.19	Ref. [171]
	Bi_2WO_6	Electrodeposition+ Thermal treatment	2.8 eV	300 W xenon lamp AM 1.5 G	−0.02- 0.27 vs. RHE	0.05 M H_2SO_4 (1)	~0.30	Ref. [172]
	α-$SnWO_4$	Hydrothermal conversion	~2.2	Xe lamp AM 1.5 G	~−0.06 vs. RHE	0.5 M KPi (7)	~0.08	Ref. [174]
Tungstates & Molybdates	Fe_2WO_6	Spray pyrolysis	~2.1	300 W Xe lamp AM 1.5 G	~0.65 vs. RHE	0.1 M KOH	~0.07	Ref. [175]
	$NiWO_4$	Hydrothermal+ Thermal treatment	~2.2	500 W Xe lamp	~-0.45 vs. Ag/AgCl	/	/	Ref. [176]
	$ZnWO_4$	Dispensing	3.3	150 W xenon lamp	−0.17 vs. RHE	0.1 M Na_2SO_4 (7)	~0.017	Ref. [177]
	$CdWO_4$	Solvothermal	~3.95	CHF-XM-500W	/	/	/	Ref. [178]
	Bi_2MoO_6	Electrodeposition+ Thermal treatment	2.6	150 W Xe lamp AM 1.5 G	~0.3 V vs. RHE	0.1 M KPi (7)	~0.065	Ref. [214]
	$Bi_2Mo_2O_9$	SILAR	3.2	300 W Xe lamp AM 1.5 G	~0.28 V vs. RHE	0.5 M KPi (7)	~0.020	Ref. [123]
	$Bi_2Mo_3O_{12}$	Electrodeposition+ Thermal treatment	3.0	300 W xenon lamp AM 1.5 G	0.36 V vs. RHE	0.1 M KPi (7.6)	~0.005	Ref. [179]
	$ZnFe_2O_4$	Atomic layer deposition	2.01	Xe lamp AM 1.5	0.64 vs. RHE	0.1 M NaOH	~0.26	Ref. [77]
	$SrTiO_3$	Pulsed laser deposition	3.2	Tungsten halogen lamp AM 1.5	−0.60~-0.75 V vs. Ag/AgCl	3 M KCl	~0.2	Ref. [185]
	$CaTiO_3$	Anodic oxidation+ Thermal treatment	~3.4	Mercury lamp high-pressure UV illumination	−0.32 vs. Ag/AgCl	0.5 M Na_2SO_4	~4	Ref. [186]
	$MnTiO_3$		2.83				~0.006	
	$FeTiO_3$	Pulsed laser deposition	2.83	500 W Xe lamp	/	0.1 M NaOH (13)	~0.030	Ref. [187]
Others	$CoTiO_3$		2.67				~0.038	
	$NiTiO_3$		2.89				~0.042	
	Sn_2TiO_4	Flux-mediated	~1.55	300 W Xe lamp AM 1.5 G	~-0.46 vs. RHE	0.5 M Na_2SO_4	~0.018	Ref. [188]
	$CuFe_2O_4$	Electrodeposition+ Thermal treatment	~1.9	450 W Xe lamp AM 1.5 G	0.8 vs. RHE	0.1 M NaOH	~0.0007	Ref. [189]
	$BiFeO_3$	Solid-state reaction	~2.6	150 W Xe lamp AM 1.5 G	~-0.2 vs. RHE	0.5 M Na_2SO_4 (pH 5.67)	/	Ref. [190]
	$CuSnO_3$	Spin-coating	~2.3	Model 94011A AM 1.5 G	0.21 vs. RHE	0.1 M Na_2SO_4 (6.5)	~0.06	Ref. [191]

[a] All photocurrent densities are relative to the potential of 1.23 V vs. RHE.

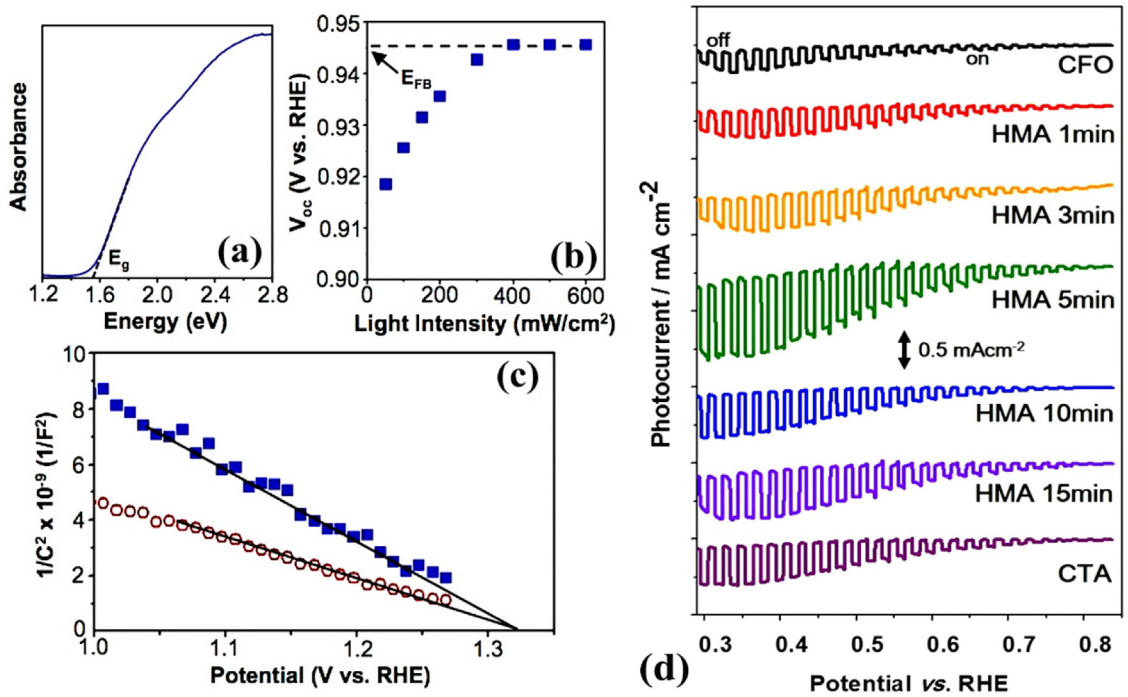

Fig. 12. (a) UV–vis-NIR absorption spectrum, (b) open circuit photovoltage (V_{oc}) measurement with varying light intensity, and (c) Mott-Schottky plots at 5 kHz (○) and 10 kHz (■) of crystalline $CuFeO_2$ film measured in 1 M NaOH. Reprinted by permission from *Ref.* [193], Copyright of 2012, the American Chemical Society. (d) Current (*J*) - potential (*V*) curves recorded with the photocathodes of untreated $CuFeO_2$ (CFO), and post-treated CFO by hybrid microwave annealing (HMA) for different durations of 1, 3, 5, 10 and 15 min. For the control, the CFO was post-treated by conventional thermal annealing (CTA). The photoreduction was performed in 1 M NaOH electrolyte. Reprinted by permission from *Ref.* [195], Copyright of 2016, the American Chemical Society.

Table 3
Key material properties and PEC activity parameters of ternary metal oxides that have been identified as photocathodes for solar water reduction.

Ternary metal oxide	Synthetic method	Band gap (eV)	Light source and filter	Flat-band potential	Electrolyte and pH	Photocurrent (mA/cm^2)	Reference
$CuBi_2O_4$	Electrodeposition	~1.8	100 W Xe lamp AM1.5 G	1.05 vs. RHE	Na_2SO_4 (10.8)	~0.045 at 0.7 vs. RHE	Ref. [196]
	Drop-casting	1.6-1.8	WACOM AM1.5 G	1.26-1.43 vs. RHE	0.2 M KP_i (6.6)	~0.3 at 0.4 vs. RHE	Ref. [197]
$CuFeO_2$	Electrodeposition	1.55	300 W Xe lamp AM1.5 G	0.98-1.3 vs. RHE	1 M NaOH	~0.085 at 0.6 vs. RHE	Ref. [193]
	Sol-gel	1.47	450 W Xe lamp AM1.5 G	1.05 vs. RHE	1 M NaOH	0.025 at 0.4 vs. RHE	Ref. [194]
$CuFe_2O_4$	Hydrothermal	1.42	150 W Xe lamp	0.14 vs. RHE	0.2 M Na_2SO_4 (~6)	0.0004 at 0 V vs. RHE	Ref. [202]
$CaFe_2O_4$	Solution method	1.9 eV	500 W Xe lamp	1.3 vs. RHE	1 M NaOH	~0.085 at -0.8 vs. Ag/AgCl	Ref. [203]
$NiFe_2O_4$	Sol-gel method	1.56	500W halogen lamp.	−0.18 V vs. SCE	0.1 M KCl (~7)	~0.030 at 0 V vs. RHE	Ref. [204]
$CuNbO_3$	Solid-state reaction	~2.0	400 W Xe lamp	/	0.5 M Na_2SO_4	~0.2 at -0.6 V vs. SCE	Ref. [205]
$CuCrO_2$	Sol-gel method	3.15	Ozone-free Xe-arc lamp	~1.1 V vs. RHE	0.1 M NaOH	~0.5 at 0.4 V vs. RHE	Ref. [206]
$CuRhO_2$	Solid-state reaction	~1.9	75 W PTI xenon arc lamp	0.4 V vs. SCE	1 M NaOH	~2 at -1.0 V vs. SCE	Ref. [207]
$CuYO_2$	Solid-state reaction	~3.5	200W Xenon lamp	0.17 V vs. SCE	1 M KOH (13.4)	~0.003 at -0.4 V vs. SCE	Ref. [208]
$CuGaO_2$	Hydrothermal	3.91	300 W Xe lamp	0.23 V vs. Ag/AgCl	0.1 M acetonitrile	0.030 at -1.2 V vs. Ag/AgCl	Ref. [209]
$CuMnO_2$	Solid-state reaction	1.31	650 Whalogen lamp	−0.26V vs. SCE	0.5 M KOH	0.0002 at -0.1 V vs. SCE	Ref. [210]
$AgRhO_2$	Ceramic method	1.7	75 W PTI xenon arc lamp 465 nm LED	0.51 V vs.Ag/AgCl	0.5 M KNO_3 (0)	9 at 0 V vs. RHE	Ref. [201]
$PbMoO_4$	Drop-casting	3.2	Xe lamp	/	0.1 M Na_2SO_4 +0.2 M KPi	~0.085 at 0 V vs. Ag/AgCl	Ref. [211]

(FDCA) can be synthesized through the oxidation of HMF, and is used as a monomer to generate polyethylene terephthalate and poly(ethylene 2,5-furandicarboxylate). In the traditional oxidation method of HMF into FDCA, Au, Pd, and Pt, or their bimetallic alloys, serve as catalysts to drive the reaction in an alkaline aqueous solution (pH ≥ 13) under high-pressure O_2 or air (3–20 bar) and at high temperature (30–130 °C) [219,220]. Inspired by several previous studies on the electrochemical oxidation of HMF into FDCA [221,222], Choi's group investigated the PEC oxidation of HMF into FDCA on a $BiVO_4$ photoanode [223]. The related reactions in their $BiVO_4$-based PEC cell for the oxidation of HMF into FDCA are shown in Fig. 14. 2, 2, 6, 6-tetramethylpiperidine 1-oxyl (TEMPO) was added into the electrolyte as a redox mediator to induce the oxidation of HMF into FDCA. Under sunlight illumination, photoexcited holes and electrons were generated in the valance and conduction bands of $BiVO_4$, respectively. The photoexcited holes firstly

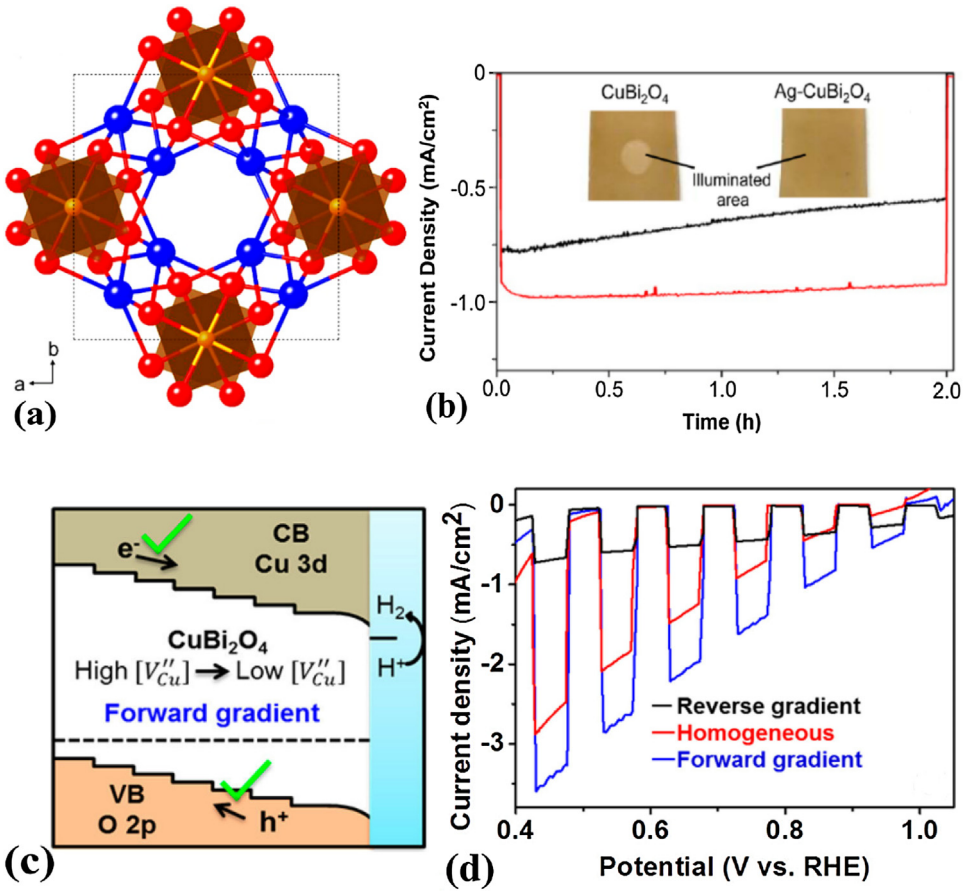

Fig. 13. (a) Drawings of the $CuBi_2O_4$ crystal structure as viewed along the c-axis. Bi, Cu, and O atoms are represented by blue, orange, and red spheres, respectively. Reprinted by permission from *Ref.* [197], Copyright of 2016, the American Chemical Society. (b) *J-t* plots at 0.6 V *vs.* RHE of $CuBi_2O_4$ (black) and Ag-$CuBi_2O_4$ (red) measured in 0.1 M NaOH solution (pH 12.8) saturated with O_2 under AM 1.5 G (100 mW/cm^2) illumination. The inset shows photographs of $CuBi_2O_4$ and Ag-$CuBi_2O_4$ electrodes after the *J-t* measurement. Reprinted by permission from *Ref.* [199], Copyright of 2016, the American Chemical Society. (c) The formation of $CuBi_2O_4$ with forward gradient. (d) Chopped LSV scans for $CuBi_2O_4$ photocathodes synthesized to a thickness of ~270 nm with uniform composition (homogeneous) or with gradient self-doping (forward and reverse). The LSV measurements were performed in 0.3 M K_2SO_4 and 0.2 M phosphate buffer (pH 6.65) with H_2O_2 under back illumination. Reprinted by permission from *Ref.* [200], Copyright of 2017, the American Chemical Society.

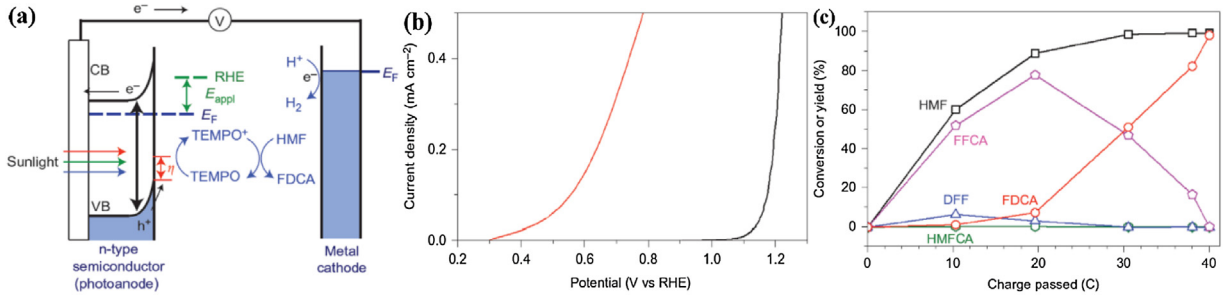

Fig. 14. (a) Schematic diagram of photoelectrochemical TEMPO-mediated HMF oxidation into FDCA. (b) LSVs of a $BiVO_4$ photoanode obtained under AM 1.5 G illumination (100 mW cm^{-2}) (orange line) and a Au electrode in the dark (black line) in a 0.5 M borate buffer solution (pH 9.2) containing 5 mM HMF and 7.5 mM TEMPO. (c) Conversion and yield (%) changes of HMF and its oxidation products during TEMPO-mediated photooxidation of HMF at 1.04 V versus RHE in a 0.5 M borate buffer solution containing 5 mM HMF and 7.5 mM TEMPO under AM 1.5 G illumination (100 mW cm^{-2}). Reprinted by permission from *Ref.* [223], Copyright of 2015, Nature Publishing Group.

drove the oxidation of TEMPO into TEMPO$^+$, and then HMF was oxidized into FDCA through the TEMPO$^+$-mediated reaction. Meanwhile, the photoexcited electrons were directionally transferred to the Pt cathode for the hydrogen evolution reaction. The TEMPO-mediated HMF oxidation was more favorable than water oxidation, both in terms of thermodynamics and kinetics. Significantly, the TEMPO-mediated PEC oxidation of HMF on a $BiVO_4$ photoanode can be performed at room temperature in a weak alkaline aqueous medium (pH 9.2). This reaction can increase the efficiency of H_2 production on the cathode. Thus, compared with the traditional oxidation method, the TEMPO-mediated PEC oxidation of HMF on a $BiVO_4$ photoanode exhibits obvious superiority with respect to reaction condition, cost, and added value of products. In our recent work, we investigated the feasibility of PEC synthesis of 5,5′-azotetrazolate energetic salts using a $BiVO_4$ photoanode [224]. Our work aimed to overcome the disadvantages of the conventional synthetic approach of 5,5′-azotetrazolate energetic salts, in which potassium permanganate ($KMnO_4$) is used as an oxidizer to drive the coupling reaction of 5-amino-1H-tetrazole at a relatively high temperature (>60 °C) [224]. Due to the formation of

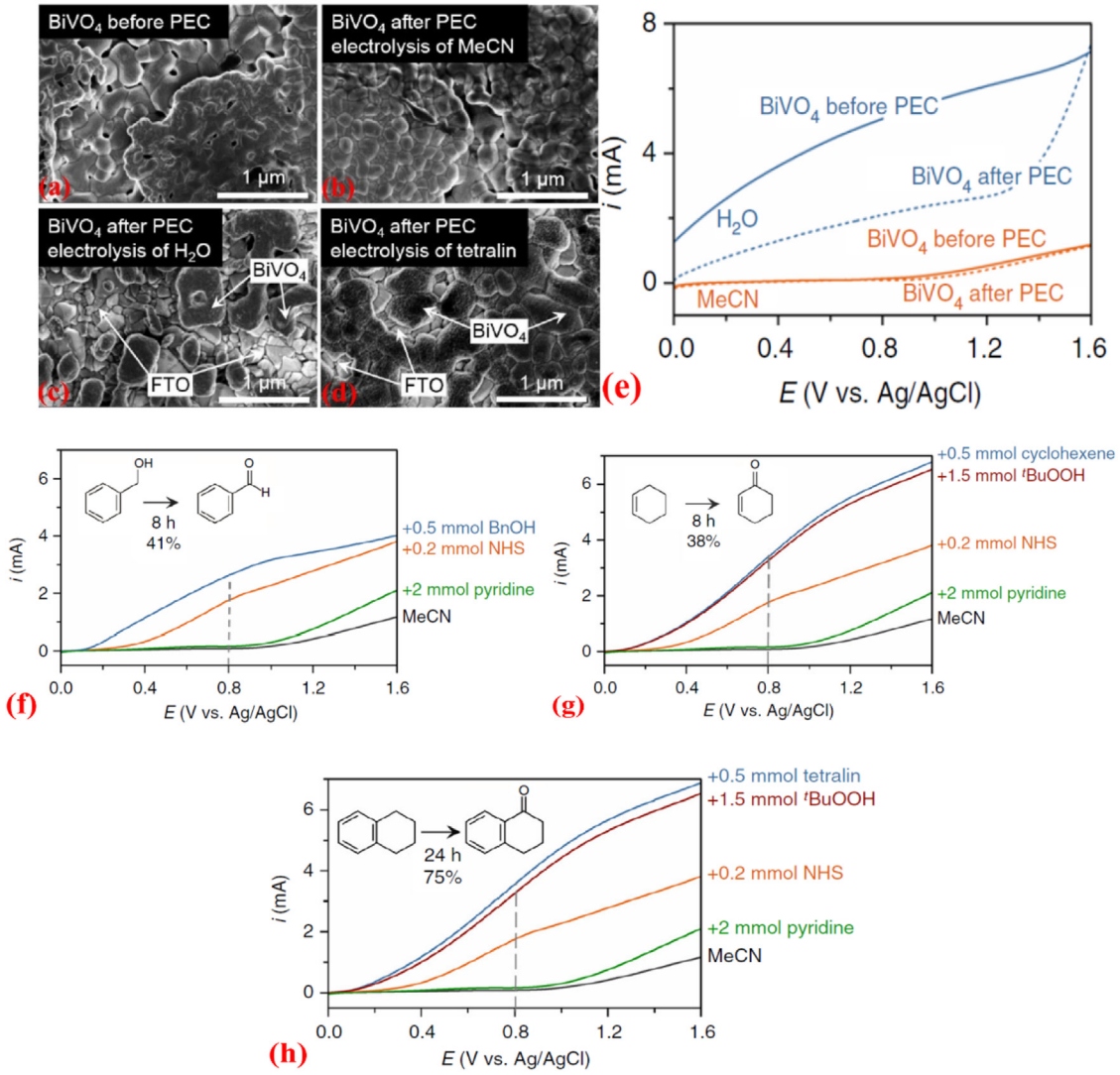

Fig. 15. (a)-(d) SEM images of $BiVO_4$ film on FTO before and after 96 h PEC electrolysis of H_2O, MeCN or tetralin. (e) Photocurrents of $BiVO_4$ photoanodes before (solid line) and after (dashed line) 96 h of PEC electrolysis in H_2O (blue) or MeCN (orange). (f)-(h) LSV curves of PEC organic oxidation profiles. Photocurrents correspond to PEC oxidations of benzyl alcohol to benzaldehyde (f), cyclohexene to cyclohexanone (g), and tetralin to 1-tetralone (h) using a $BiVO_4$ photoanode immersed in 25 mL MeCN containing 0.1 M $LiClO_4$ and subjected to AM1.5 G light. Reprinted by permission from *Ref.* [226], Copyright of 2015, Nature Publishing Group.

the MnO_2 by-product, the purification of 5,5′-azotetrazolate energetic salts is time consuming. Moreover, the production safety of 5,5′-azotetrazolate energetic salts could be compromised owing to the heated reaction, with a risk of explosion accidents. Our results indicated that the photogenerated holes of $BiVO_4$ can directly drive the coupling reaction of 5-amino-*1H*-tetrazole to form 5,5′-azotetrazolate energetic salts at room temperature without the production of any by-products.

For PEC organic synthesis on photoelectrodes, the selection of solvent requires consideration. Firstly, the polarity of the solvent influences the solubility of the organic substrate and supporting electrolyte. Secondly, a degradation reaction of the solvent can disrupt the desired organic reaction on the photoelectrode. Lastly, the stability of the photoelectrode is closely related to the solvent. In the work of Li et al. [226], the PEC oxidation of benzyl alcohol, cyclohexene, and tetralin into their corresponding carbonyl compounds was studied in a $BiVO_4$ photoanode-containing cell using different solvent-electrolyte combinations. They found that the photocorrosion of $BiVO_4$ photoanode in MeCN is much lower than that in H_2O, which is an outstanding property for PEC organic synthesis (as shown in Fig. 15). In addition, their results confirmed that the PEC oxidation of benzyl alcohol, cyclohexene, and tetralin into their corresponding carbonyl compounds can only be achieved in MeCN (solvent)-$LiClO_4$ (electrolyte) with pyridine/N-hydroxysuccinimide as the redox mediator; other solvents (such as, acetone and CH_3NO_2) and electrolytes (such as, Bu_4NClO_4 and Bu_4NPF_6) did not yield the desired products. Another factor that requires particular attention in PEC organic synthesis is the photoelectrode material. In essence, the fundamental properties of the photoelectrode material determine the reaction selectivity and activity of organic compounds. In particular, the PEC oxidation and reduction properties of semiconductor photoelectrodes strongly depend on their band gap characteristic. Tateno et al. described the PEC dimethoxylation of furan with methanol on a $BiVO_4/WO_3$ photoanode through the formation of Br^+/Br^- redox mediator in MeCN (solvent)-Et_4NBF_4 (electrolyte) [227]. They demonstrated that WO_3 and TiO_2 photoanodes are unreactive for the PEC dimethoxylation of furan with methanol under the same conditions. Similar observations that different photoelectrodes are of obvious selectivity for PEC organic reaction have also been reported by Bai et al. [228] and Zhang et al. [229]. In addition to the solvent and photoelectrode material, the influence of the redox mediator on PEC

organic synthesis should not be ignored. In principle, the redox mediator can connect the transfer of charge between the photoelectrode and organic substrate in an indirect reaction. For example, TEMPO/TEMPO$^+$ is a known redox mediator that selectively oxidizes primary alcohols over secondary alcohols in basic conditions [230]. Br^+/Br^- redox can mediate the cleavage of C-Br and C—CI bonds in MeCN [231]. In several reported studies of PEC organic synthesis, a suitable redox mediator was reported to play a key role in the formation of the desired product [223–225]. Of course, some organic synthesis reactions can be directly driven by the photogenerated charge of the semiconductor photoelectrode. Typically, aniline can be photoelectrochemically reduced to form nitrobenzene on a Cu_2ZnSnS_4 electrode [232]. Further, cyclohexanol and cyclohexanone can be directly photoelectrochemically obtained through the C–H bond activation of cyclohexane on a WO_3 photoanode [233].

In general, PEC organic synthesis is a new concept of converting sunlight into valuable chemical products, and has indeed been demonstrated in several PEC systems. There are various scientific problems that need to be addressed for the development of large-scale and cost-effective applications. Similar to the development direction of PEC water splitting, once high-efficiency ternary metal oxide photoelectrodes are developed, it will be possible to utilize PEC organic synthesis in practical applications.

Conclusion and outlook

In this review, recent advances in the use of ternary metal oxides as photoelectrode materials for water splitting and organic synthesis are summarized and discussed. We have introduced the fundamental properties, PEC performance limitations and application challenges of ternary metal oxides, and have highlighted the recently proposed strategies for improving the PEC performance of ternary metal oxide photoelectrodes. As discussed, although several challenges (such as, poor charge separation and transfer, inaccurate and complicated synthesis) exist for ternary metal oxides, the recent advances in ternary metal oxide photoelectrodes demonstrate their potential application prospects in PEC water splitting and organic synthesis. From these encouraging results, it is expected that more ternary metal oxide photoelectrodes with high performance be developed and investigated for water splitting and organic synthesis. For the achievement of expected PEC water splitting and organic synthesis, the following directions should be considered overall in the future research of ternary metal oxide photoelectrodes.

(1) To find the efficient ternary metal oxide photoelectrodes from the vast candidates quickly, the research of high throughput identification and screening methods, particularly the combination method of experimental investigation and computational prediction is of great importance. In addition, it is necessary to build a standard database for providing the band gap, band positions, photoactive phase data of the ternary metal oxides based on the identification and screening results. Those works would promote the discovery and study of ternary metal oxide photoelectrodes.
(2) To achieve more effective water splitting and organic synthesis on the ternary metal oxide photoelectrodes, their properties of light harvesting, charge separation and surface reaction should be taken an integral consideration. Meanwhile, the performance-determined factor of specific ternary metal oxide photoelectrodes should be carefully investigated so as to modify the photoelectrodes. Strategically, the as-developed research approaches and techniques on binary metal oxide photoelectrodes have important enlightenment and reference significance for ternary metal oxide photoelectrodes. In addition, the PEC organic synthesis on ternary metal oxide photoelectrodes includes more complicated kinetic mechanism than PEC water splitting. To ascertain the related scientific problems, it is necessary to pay close attention and take reference to the research of electrochemical synthesis of organics.
(3) For the practical PEC water splitting and organic synthesis, the requirements of for the ternary metal oxide photoelectrodes not only include high activity, but also acceptable stability. Most modification studies to date have focused on the improvement in PEC activity of ternary metal oxide photoelectrodes; there are fewer studies of modification to their PEC stability. It is important to investigate the electrolyte/ternary metal oxide photoelectrode interface in more details; this would increase our understanding of the PEC stability of ternary metal oxide photoelectrodes. In particular, the influence of the kinetic pathway of PEC water splitting and organic synthesis on the thermodynamic dissolution of ternary metal oxide photoelectrodes should be analyzed.

In all, the discussion of ternary metal oxide photoelectrodes in our review is not exhaustive. We hope that this review will provide valuable information and inspiration for the study of water splitting and organic synthesis on ternary metal oxide photoelectrodes in the future.

Declaration of Competing Interest

The authors declare no conflicts of interest exist.

Acknowledgements

The authors thank the support of National Natural Science Foundation of China (41702037, 41831285, and 21773114), Sichuan Science and Technology Program (2017JY0146).

References

[1] O. Coddington, J.L. Lean, P. Pilewskie, M. Snow, D. Lindholm, Bull. Amer. Meteor. Soc. 163 (2016) 1265–1282.
[2] [dataset] International Energy Agency, Key World Energy Statistics 2017, International Energy Agency (2017).
[3] T. Jackson, M. Oliver, Energy Policy 28 (2000) 983–988.
[4] J. Phillips, Renewable Sustainable Energy Rev. 27 (2013) 435–444.
[5] A. Kudo, Y. Miseki, Chem. Soc. Rev. 38 (2009) 253–278.
[6] W. Tu, Y. Zhou, Z. Zou, Adv. Mater. 26 (2014) 4607–4626.
[7] M. Thirugnanasambandam, S. Iniyan, R. Goic, Renewable Sustainable Energy Rev. 14 (2010) 312–322.
[8] L.M. Reid, T. Li, Y. Cao, C.P. Berlinguette, Sustain. Energy Fuels 2 (2018) 1905–1927.
[9] M. Grätzel, Nature 414 (2001) 338–344.
[10] H. Hao, L. Zhang, W. Wang, S. Zeng, Catal. Sci. Technol. 8 (2018) 1229–1250.
[11] H. Dotan, K. Sivula, M. Grätzel, A. Rothschild, S.C. Warren, Energy Environ. Sci. 4 (2011) 958–964.
[12] K.R. Reyes-Gil, D.B. Robinson, ACS Appl. Mater. Inter. 5 (2013) 12400–12410.
[13] Z. Wang, L. Wang, Chinese J. Catal. 39 (2018) 369–378.
[14] M.C. Toroker, D.K. Kanan, N. Alidoust, L.Y. Isseroff, P. Liao, E.A. Carter, Phys. Chem. Chem. Phys. 13 (2011) 16644–16654.
[15] Z.M. Adriana, Metal Oxide-based Photocatalysis: Fundamentals and Prospects for Application, Elsevier, San Diego, California, 2018.
[16] F.F. Abdi, S.P. Berglund,J. Phys. D Appl. Phys. 50 (2017), 193002.
[17] D.K. Lee, D. Lee, M.A. Lumley, K.S. Choi, Chem. Soc. Rev. 48 (2019) 2126–2157.
[18] Z.B. Chen, T.F. Jaramillo, T.G. Deutsch, A. Kleiman-Shwarsctein, A.J. Forman, N. Gaillard, R. Garland, K. Takanabe, C. Heske, M. Sunkara, E.W. McFarland, K. Domen, E.L. Miller, J.A. Turner, H.N. Dinh, J. Mater. Res. 25 (2010) 3–16.
[19] K. Sivula, Chimia 67 (2013) 155–161.
[20] M.G. Walter, E.L. Warren, J.R. McKone, S.W. Boettcher, Q. Mi, E.A. Santori, N.S. Lewis, Chem. Rev. 110 (2010) 6446–6473.
[21] Q. Jia, K. Iwashina, A. Kudo, Proc. Natl. Acad. Sci. U. S. A. 109 (2012) 11564–11569.
[22] A. Walsh, Y. Yan, M.N. Huda, M.M. Al-Jassim, S.H. Wei, Chem. Mater. 21 (2009) 547–551.

[23] X. Yang, X. Liana, S. Liu, C. Jiang, J. Tian, G. Wang, J. Chen, R. Wang, Appl. Surf. Sci. 282 (2013) 538–543.
[24] A.J. Rettie, W.D. Chemelewski, D. Emin, C.B. Mullins, J. Phys. Chem. Lett. 7 (2016) 471–479.
[25] M. Ziwritsch, S. Müller, H. Hempel, T. Unold, F.F. Abdi, R. van de Krol, D. Friedrich, R. Eichberger, ACS Energy Lett. 1 (2016) 888–894.
[26] D.K. Lee, K.S. Choi, Nat. Energy 3 (2018) 53–60.
[27] T.S. Sinclair, B.M. Hunter, J.R. Winkler, H.B. Gray, A.M. Müller, Mater. Horiz. 2 (2015) 330–337.
[28] S. Byun, G. Jung, S.Y. Moon, B. Kim, J.Y. Park, S. Jeon, S.W. Nam, B. Shin, Nano Energy 43 (2018) 244–252.
[29] J. Song, K.S. Choi, M.J. Seo, Y.R. Jo, J. Lee, T.L. Kim, S.Y. Jeong, H. An, H.W. Jang, B.J. Kim, C. Jeon, S. Lee, Chem. Mater. 30 (2018) 5673–5681.
[30] M.D. Casper, M.D. Losego, J.P. Maria, J. Mater. Sci. 48 (2013) 1578–1584.
[31] W.J. Yin, H. Tang, S.H. Wei, M.M.A. Jassim, J. Turner, Y.F. Yan,Phys. Rev. B 82 (2010), 045106.
[32] H.M. Chen, C.K. Chen, R.S. Liu, L. Zhang, J. Zhang, D.P. Wilkinson, Chem. Soc. Rev. 41 (2012) 5654–5671.
[33] A.J.E. Rettie, H.C. Lee, L.G. Marshall, J.F. Lin, C. Capan, J. Lindemuth, J.S. McCloy, J. Zhou, A.J. Bard, C.B. Mullins, J. Am. Chem. Soc. 135 (2013) 11389–11396.
[34] H.S. Park, K.E. Kweon, H. Ye, E. Paek, G.S. Hwang, A.J. Bard, J. Phys. Chem. C 115 (2011) 17870–17879.
[35] W. Luo, Z. Yang, Z. Li, J. Zhang, J. Liu, Z. Zhao, Z. Wang, S. Yan, T. Yu, Z. Zou, Energy Environ. Sci. 4 (2011) 4046–4051.
[36] W.J. Yin, S.H. Wei, M.M.A. Jassim, J. Turner, Y. Yan,Phys. Rev. B 83 (2011), 155102.
[37] S.P. Berglund, A.J.E. Rettie, S. Hoang, C.B. Mullins, Phys. Chem. Chem. Phys. 14 (2012) 7065–7075.
[38] K.P.S. Parmar, H.J. Kang, A. Bist, P. Dua, J.S. Jang, J.S. Lee, ChemSusChem 5 (2012) 1926–1934.
[39] F.F. Abdi, T.J. Savenije, M.M. May, B. Dam, R. van de Krol, J. Phys. Chem. Lett. 4 (2013) 2752–2757.
[40] Y. Zhang, Z. Yi, G. Wu, Q. Shen, J. Photochem. Photobiol. A: Chem. 327 (2016) 25–32.
[41] X. Zhong, H. He, M. Yang, G. Ke, Z. Zhao, F. Dong, B. Wang, Y. Chen, X. Shi, Y. Zhou, J. Mater. Chem. A 6 (2018) 10456–10465.
[42] J. Lee, H. Ye, S. Pan, A.J. Bard, Anal. Chem. 19 (2008) 7445–7450.
[43] S.P. Berglund, H.C. Lee, P.D. Nunez, A.J. Bard, C.B. Mullins, Phys. Chem. Chem. Phys. 15 (2013) 4554–4565.
[44] C. Bhattacharya, H. Chan Lee, A.J. Bard, J. Phys. Chem. C 117 (2013) 9633–9640.
[45] W. Shi, N. Chopra, Nanomater. Energy 2 (2013) 256–264.
[46] M. Zhang, J. Lee, L. Wang, Q. Duan, J. Zhang, H. Qi, Chemcatchem 7 (2015) 3978–3984.
[47] J. Ding, J. Bao, S. Sun, Z. Luo, C. Gao, J. Comb. Chem. 11 (2009) 523–526.
[48] H. Zhang, J.J. Wang, J. Fan, Q. Fang, Talanta 116 (2013) 946–950.
[49] Y. Wu, P. Lazic, G. Hautier, K. Persson, G. Ceder, Energy Environ. Sci. 6 (2013) 157–168.
[50] X. Zhang, Z. Zhang, D. Wu, X. Zhang, X. Zhao, Z. Zhou,Small Methods 2 (2018), 1700359.
[51] S. Kawasaki, K. Nakatsuji, J. Yoshinobu, F. Komori, R. Takahashi, M. Lippmaa, K. Mase, A. Kudo,Appl. Phys. Lett. 101 (2012), 033910.
[52] D. Bohra, W.A. Smith, Phys. Chem. Chem. Phys. 17 (2015) 9857–9866.
[53] N. Rong, M. Chu, Y. Tang, C. Zhang, X. Cui, H. He, Y. Zhang, P. Xiao, J. Mater. Sci. 51 (2016) 5712–5723.
[54] Y. Guo, N. Zhang, X. Wang, Q. Qian, S. Zhang, Z. Li, Z. Zou, J. Mater. Chem. A Mater. Energy Sustain. 5 (2017) 7571–7577.
[55] S. Piskunov, O. Lisovski, J. Begens, D. Bocharov, Y.F. Zhukovskii, M. Wessel, E. Spohr, J. Phys. Chem. C 119 (2015) 18686–18696.
[56] N. Singh, U. Schwingenschlögl, EPL-Europhys. Lett. 104 (2013) 37002.
[57] K. Lai, Y. Zhu, J. Lu, Y. Dai, B. Huang, Comp. Mater. Sci. 67 (2013) 88–92.
[58] K. Lai, Y. Zhu, J. Lu, Y. Dai, B. Huang, Solid State Sci. 24 (2013) 79–84.
[59] P. Li, X. Zhao, H. Sun, L. Wang, B. Song, B. Gao, W. Fan, RSC Adv. 6 (2016) 74483–74492.
[60] L. Jiang, Q. Wang, C. Li, J. Yuan, W. Shangguan, Int. J. Hydrogen Energy 35 (2010) 7043–7050.
[61] K.M. Parida, S. Martha, D.P. Das, N. Biswal, J. Mater. Chem. 20 (2010) 7144–7149.
[62] A. Mukherji, C. Sun, S.C. Smith, G.Q. Lu, L. Wang, J. Phys. Chem. C 115 (2011) 15674–15678.
[63] S. Kumar, S. Tonda, A. Baruah, B. Kumarb, V. Shanker, Dalton Trans. 43 (2014) 16105–16114.
[64] W.J. Jo, J.W. Jang, K.J. Kong, H.J. Kang, J.Y. Kim, H. Jun, K.P.S. Parmar, J.S. Lee, Angew. Chem. Int. Ed. 51 (2012) 3147–3151.
[65] B. Anke, M. Rohloff, M.G. Willinger, W. Hetaba, A. Fischer, M. Lerch, Solid State Sci. 63 (2017) 1–8.
[66] G. Wang, Y. Yang, D. Han, Y. Li, Nano Today 13 (2017) 23–39.
[67] G.M. Wang, Y.C. Ling, Y. Li, Nanoscale 4 (2012) 6682–6691.
[68] G. Wang, Y. Ling, X. Lu, F. Qian, Y. Tong, J.Z. Zhang, V. Lordi, C.R. Leao, Y. Li, J. Phys. Chem. C 117 (2013) 10957–10964.
[69] S. Wang, P. Chen, Y. Bai, J.H. Yun, G. Liu, L. Wang,Adv. Mater. 30 (2018), 1800486.
[70] T.W. Kim, Y. Ping, G.A. Galli, K.S. Choi, Nat. Commun. 6 (2015) 8769.
[71] J. Wu, Y. Chen, L. Pan, P. Wang, Y. Cui, D. Kong, L. Wang, X. Zhang, J. Zou, Appli. Catal. B- Environ. 221 (2018) 187–195.
[72] B. Zhang, L. Wang, Y. Zhang, Y. Ding, Y. Bi, Angew. Chem. Int. Ed. 57 (2018) 2248–2252.
[73] Y. Tang, N. Rong, F. Liu, M. Chu, H. Dong, Y. Zhang, P. Xiao, Appl. Surf. Sci. 361 (2016) 133–140.
[74] W. Guo, Z. Duan, O. Mabayoje, W.D. Chemelewski, P. Xiao, G. Henkelman, Y. Zhang, C.B. Mullins, J. Electrochem. Soc. 163 (2016) H970–H975.
[75] Z. Ma, O. Linnenberg, A. Rokicinska, P. Kustrowski, A. Slabon, J. Phys. Chem. C 122 (2018) 19281–19288.
[76] J.H. Kim, Y.J. Jang, J.H. Kim, J.W. Jang, S.H. Choi, J.S. Lee, Nanoscale 7 (2015) 19144–19151.
[77] J.H. Kim, Y.J. Jang, S.H. Choi, B.J. Lee, J.H. Kim, Y.B. Park, C.M. Nam, H.G. Kim, J.S. Lee, J. Mater. Chem. A Mater. Energy Sustain. 6 (2018) 12693–12700.
[78] W. Ye, F. Chen, F. Zhao, N. Han, Y. Li, ACS Appl. Mater. Inter. 8 (2016) 9211–9217.
[79] D. Hu, P. Diao, Xu Di, M. Xia, Y. Gu, Q. Wu, C. Li, S. Yang, Nanoscale 8 (2016) 5892–5901.
[80] M. Zhou, Z. Liu, X. Li, Z. Liu, Ind. Eng. Chem. Res. 57 (2018) 6210–6217.
[81] G. Dong, Y. Zhang, W. Wang, L. Wang, Y. Bi, Energy Technol. 5 (2017) 1912–1918.
[82] A.G. Hufnagel, K. Peters, A. Müller, C. Scheu, D.F. Rohlfing, T. Bein, Adv. Funct. Mater. 26 (2016) 4435–4443.
[83] X. Zhu, N. Guijarro, Y. Liu, P. Schouwink, R.A. Wells, F.L. Formal, S. Sun, C. Gao, K. Sivula,Adv. Mater. 30 (2018), 1801612.
[84] H.X. Dang, A.J.E. Rettie, C.B. Mullins, J. Phys. Chem. C 119 (2015) 14524–14531.
[85] S.P. Berglund, D.W. Flaherty, N.T. Hahn, A.J. Bard, C.B. Mullins, J. Phys. Chem. C 115 (2011) 3794–3802.
[86] K.J. McDonalda, K.S. Choi, Energy Environ. Sci. 5 (2012) 8553–8557.
[87] H. He, S.P. Berglund, A.J.E. Rettie, W.D. Chemelewski, P. Xiao, Y. Zhang, C.B. Mullins, J. Mater. Chem. A Mater. Energy Sustain. 2 (2014) 9371–9379.
[88] E. Alarcón-Lladó, L. Chen, M. Hettick, N. Mashouf, Y. Lin, A. Javey, J.W. Ager, Phys. Chem. Chem. Phys. 16 (2014) 1651–1657.
[89] D. Peeters, O.M. Reyes, L. Mai, A. Sadlo, S. Cwik, D. Rogalla, H.W. Becker, H.M. Schütz, J. Hirst, S. Müller, D. Friedrich, D. Mitoraj, M. Nagli, M. Caspary Toroker, R. Eichberger, R. Beranek, A. Devi, J. Mater. Chem. A Mater. Energy Sustain. 6 (2018) 10206–10216.
[90] J. Zhang, T. Wang, X. Chang, A. Li, J. Gong, Chem. Sci. 7 (2016) 6381–6386.
[91] T. Yao, X. An, H. Han, J.Q. Chen, C. Li,Adv. Energy Mater. 8 (2018), 1800210.
[92] A. Fujishima, T.N. Rao, D.A. Tryk, J. Photochem. Photobiol. C Photochem. Rev. 1 (2000) 1–21.
[93] Z. Zhang, J.T. Yates Jr, Chem. Rev. 112 (2012) 5520–5551.
[94] M. Liu, J.L. Lyons, D. Yan, M.S. Hybertsen, Adv. Funct. Mater. 26 (2016) 219–225.
[95] J. Su, C. Liu, D. Liu, M. Li, J. Zhou, ChemCatChem 8 (2016) 1–9.
[96] B. Zhang, H. Zhang, Z. Wang, X. Zhang, X. Qina, Y. Dai, Y. Liu, P. Wang, Y. Li, B. Huang, Appl. Catal. B-Environ. 211 (2017) 258–265.
[97] M. Klusackova, R. Nebel, K.M. Macounova, M. Klementova, P. Krtil, Electrochim. Acta 297 (2019) 215–222.
[98] J. Ran, J. Zhang, J. Yu, M. Jaroniec, S.Z. Qiao, Chem. Soc. Rev. 43 (2014) 7787–7812.
[99] D. Li, J.Y. Shi, C. Li,Small 14 (2018), 1704179.
[100] T.W. Kim, K. Choi, Science 343 (2014) 990–994.
[101] F. Tang, W. Cheng, H. Su, X. Zhao, Q. Liu, ACS Appl. Mater. Inter. 10 (2018) 6228–6234.
[102] G. Dong, H. Hu, L. Wang, Y. Zhang, Y. Bi, J. Catal. 366 (2018) 258–265.
[103] K.M. Nam, E.A. Cheon, W.J. Shin, A.J. Bard, Langmuir 39 (2015) 10897–10903.
[104] C.E. Creissen, J. Warnan, E. Reisner, Chem. Sci. 9 (2018) 1439–1447.
[105] P.M. Rao, L. Cai, C. Liu, I.S. Cho, C.H. Lee, J.M. Weisse, P. Yang, X. Zheng, Nano Lett. 14 (2014) 1099–1105.
[106] S.J. Hong, S. Lee, J.S. Jang, J.S. Lee, Energy Environ. Sci. 4 (2011) 1781–1787.
[107] Y. Zhou, L. Zhang, L. Lin, B.R. Wygant, Y. Liu, Y. Zhu, Y. Zheng, C.B. Mullins, Y. Zhao, X. Zhang, G. Yu, Nano Lett. 17 (2017) 8012–8017.
[108] M.G. Lee, D.H. Kim, W. Sohn, C.W. Moon, H. Park, S. Lee, H.W. Jang, Nano Energy 28 (2016) 250–260.
[109] C. Liu, J. Zhou, J. Su, L. Guo, Appl. Catal. B-Environ. 241 (2019) 506–513.
[110] L. Xia, J. Bai, J. Li, Q. Zeng, L. Li, B. Zhou, Appl. Catal. B-Environ. 204 (2017) 127–133.
[111] A.P. Singh, N. Kodan, B.R. Mehta, A. Held, L. Mayrhofer, M. Moseler, ACS Catal. 6 (2016) 5311–5318.
[112] S.K. Pilli, T.G. Deutsch, T.E. Furtak, L.D. Brown, J.A. Turner, A.M. Herring, Phys. Chem. Chem. Phys. 15 (2013) 3273–3278.
[113] E.S. Kim, H.J. Kang, G. Magesh, J.Y. Kim, J. Jang, J.S. Lee, ACS Appl. Mater. Inter. 6 (2014) 17762–17769.
[114] H. He, Y. Zhou, G. Ke, X. Zhong, M. Yang, L. Bian, K. Lv, F. Dong, Electrochim. Acta 257 (2017) 181–191.
[115] S.N. Lou, J. Scott, A. Iwase, R. Amal, Y.H. Ng, J. Mater. Chem. A Mater. Energy Sustain. 4 (2016) 6964–6971.
[116] L. Wang, R. Wang, Y. Zhou, Q. Shen, J. Ye, C. Wu, Z. Zou, Catal. Today (2018), http://dx.doi.org/10.1016/j.cattod.2018.11.054.
[117] J. Long, W. Wang, S. Fu, L. Liu, J. Colloid Inter. Sci. 536 (2019) 408–413.
[118] D. Wang, P.S. Bassi, H. Qi, X. Zhao, L. Gurudayal, H. Wong, R. Xu, T. Sritharan, Z. Chen, Materials 9 (2016) 348.
[119] W. Yang, B. Ma, W. Wang, Y. Wen, D. Zeng, B. Shan, Phys. Chem. Chem. Phys. 15 (2013) 19387–19394.
[120] L. Ge, C. Han, J. Liu, Appl. Catal. B-Environ. 108 (2011) 100–107.

[121] S. Xie, K. Ouyang, Y. Lao, P. He, Q. Wang, J. Colloid Inter. Sci. 493 (2017) 198–205.
[122] M.A. Mahadik, H. Chung, S. Lee, M. Cho, J.S. Jang, ACS Sustain. Chem. Eng. 6 (2018) 12489–12501.
[123] Y. Xiong, L. Yang, H. He, J. Wan, P. Xiao, W. Guo, Electrochim. Acta 264 (2018) 26–35.
[124] X. Chang, T. Wang, P. Zhang, J. Zhang, A. Li, J. Gong, J. Am. Chem. Soc. 137 (2015) 8356–8359.
[125] S. Xie, T. Zhai, Y. Zhu, W. Li, R. Qiu, Y. Tong, X. Lu, Int. J. Hydrogen Energy 39 (2014) 4820–4827.
[126] K. Li, C. Zhang, X. Li, Y. Du, P. Yang, M. Zhu, Catal. Today (2018), http://dx.doi.org/10.1016/j.cattod.2018.11.003.
[127] W. He, R. Wang, L. Zhang, J. Zhu, X. Xiang, F. Li, J. Mater. Chem. A Mater. Energy Sustain. 3 (2015) 17977–17982.
[128] J. Du, X. Zhong, H. He, Huang J, M. Yang, G. Ke, J. Wang, Y. Zhou, F. Dong, Q. Ren, L. Bian, ACS Appl. Mater. Inter. 10 (2018) 42207–42216.
[129] G. Liu, J.C. Yu, G.Q. Lu, H.M. Cheng, Chem. Commun. (Camb.) 47 (2011) 6763–6783.
[130] E.S. Jang, J.H. Won, S.J. Hwang, J.H. Choy, Adv. Mater. 18 (2006) 3309–3312.
[131] H. Tada, M. Fujishima, H. Kobayashi, Chem. Soc. Rev. 40 (2011) 4232–4243.
[132] Y.P. Xie, G. Liu, L. Yin, H.M. Cheng, J. Mater. Chem. 22 (2012) 6746–6751.
[133] Y.C. Zhang, Z. Li, L. Zhang, L. Pan, X. Zhang, L. Wang, F.E. Aleem, J.J. Zou, Appl. Catal. B-Environ. 224 (2018) 101–108.
[134] S. Wang, H. Chen, G. Gao, T. Butburee, M. Lyu, S. Thaweesak, J.H. Yun, A. Du, G. Liu, L. Wang, Nano Energy 24 (2016) 94–102.
[135] H.L. Tan, R. Amal, Y.H. Ng, J. Mater. Chem. A Mater. Energy Sustain. 5 (2017) 16498–16521.
[136] T. Liu, X. Zhou, M. Dupuis, C. Li, Phys. Chem. Chem. Phys. 17 (2015) 23503–23510.
[137] Z. Zhao, Z. Li, Z. Zou, Phys. Chem. Chem. Phys. 13 (2011) 4746–4753.
[138] J. Yang, D. Wang, X. Zhou, C. Li, Chem. Eur. J. 19 (2013) 1320–1326.
[139] M.R.D. Bomio, R.L. Tranquilin, F.V. Motta, C.A. Paskocimas, R.M. Nascimento, L. Gracia, J. Andres, E. Longo, J. Phys. Chem. C 117 (2013) 21382–21395.
[140] M. Hashim, C. Hu, X. Wang, X. Li, D. Guo, Appl. Sur. Sci. 258 (2012) 5858–5862.
[141] J. Song, M. Seo, T. Lee, Y.R. Jo, J. Lee, T. Kim, S.Y. Kim, S.M. Kim, S. Jeong, H. An, S. Kim, B. Lee, D. Lee, H. Jang, B.J. Kim, S. Lee, ACS Catal. 8 (2018) 5952–5962.
[142] H. Han, S. Shin, D. Kim, I. Park, P.S. Hang, J.K. Lee, I. Cho, X. Zheng, Energy Environ. Sci. 11 (2018) 1299–1306.
[143] M. Yang, H.A. Liao, J. Huang, Y. Tang, J. Wang, G. Ke, F. Dong, L. Yang, L. Bian, Y. Zhou, Inorg. Chem. 57 (2018) 15280–15288.
[144] W.N. Zhao, Z.P. Liu, Chem. Sci. 5 (2014) 2256–2264.
[145] B. Xin, L. Jing, Z. Ren, B. Wang, H. Fu, J. Phys. Chem. B 109 (2005) 2805–2809.
[146] C.W. Kim, Y.S. Son, M.J. Kang, D.Y. Kim, Y.S. Kang,Adv. Energy Mater. 6 (2016), 1501754.
[147] L. Xia, J. Li, J. Bai, L. Li, S. Chen, B. Zhou, Nano-Micro Lett. 1 (2018) 10–11.
[148] L. Zhang, W. Wang, S. Sun, D. Jiang, E. Gao, Appl. Catal. B-Environ. 162 (2015) 470–474.
[149] Y. Hu, G. Chen, C. Li, Y. Zhou, J. Sun, S. Hao, Z. Han, J. Mater. Chem. A Mater. Energy Sustain. 4 (2016) 5274–5281.
[150] B. Wang, S. Shen, L. GuO, Appl. Catal. B-Environ. 166-167 (2015) 320–326.
[151] J. Long, S. Wang, H. Chang, B. Zhao, B. Liu, Y. Zhou, W. Wei, X. Wang, L. Hang, Hang W, Small 10 (2014) 2791–2795.
[152] P. Li, X. Chen, H. He, X. Zhou, Y. Zhou, Z. Zou,Adv. Mater. 30 (2018), 1703119.
[153] Y. Park, K.J. McDonald, K.S. Choi, Chem. Soc. Rev. 42 (2013) 2321–2337.
[154] A. Kudo, K. Omori, H. Kato, J. Am. Chem. Soc. 121 (1999) 11459–11467.
[155] Y. Pihosh, I. Turkevych, K. Mawatari, J. Uemura, Y. Kazoe, S. Kosar, K. Makita, T. Sugaya, T. Matsui, D. Fujita, M. Tosa, M. Kondo, T. Kitamori, Sci. Rep. 5 (2015) 11141.
[156] L. Zhou, Q.M. Yan, A. Shinde, D. Guevarra, P.F. Newhouse, N. Becerra-Stasiewicz, S.M. Chatman, J.A. Haber, J.B. Neaton, J.M. Gregoire, Adv. Energy Mater. 5 (2015) 1500968.
[157] J.A. Seabold, N.R. Neale, Chem. Mater. 27 (2015) 1005–1013.
[158] W.L. Guo, W.D. Chemelewski, O. Mabayoje, P. Xiao, Y.H. Zhang, C.B. Mullins, J. Phys. Chem. C 119 (2015) 27220–27227.
[159] L. Zhou, Q.M. Yan, J.Y. Ryan, J.R. Jones, N. Becerra-Stasiewicz, S.K. Suram, A. Shinde, D. Guevarra, J.B. Neaton, K.A. Persson, J.M. Gregoire, Phys. Chem. Chem. Phys. 18 (2016) 9349–9352.
[160] M.A. Lumley, K. Choi, Chem. Mater. 29 (2017) 9472–9479.
[161] C. Jiang, M. Farmand, C.H. Wu, Y. Liu, J.H. Guo, W.S. Drisdell, J.K. Cooper, I.D. Sharp, Chem. Mater. 29 (2017) 3334–3345.
[162] Q. Yan, G. Li, P.F. Newhouse, J. Yu, K.A. Persson, J.M. Gregoire, J.B. Neaton,Adv. Energy Mater. (2015), 1401840.
[163] C.D. Morton, I.J. Slipper, M.J.K. Thomas, B.D. Alexander, J. Photochem. Photobiol. A-Chem. 216 (2010) 209–214.
[164] H. Mandal, S. Shyamal, P. Hajra, A. Bera, D. Sariket, S. Kundub, C. Bhattacharya, RSC Adv. (2015) 1–29.
[165] H. Sameie, A.A. Sabbagh Alvani, N. Naseri, F. Rosei, G. Mul, B.T. Mei, J. Electrochem. Soc. 165 (2018) H353–H359.
[166] R. Krol, J. Segalini, C.S. Enache, J. Photon. Energy 1 (2011) 016001–016010.
[167] W.D. Chemelewski, O. Mabayoje, C.B. Mullins, J. Phys. Chem. C 119 (2015) 26803–26808.
[168] C.R. Lhermitte, B.M. Bartlett, Acc. Chem. Res. 49 (2016) 1121–1129.
[169] A. Kuzmin, A. Kalinko, R.A. Evarestov, Acta Mater. 61 (2013) 371–378.
[170] K.J. Pyper, J.E. Yourey, B.M. Bartlett, J. Phys. Chem. C 117 (2013) 24726–24732.
[171] Y. Gao, T.W. Hamann, J. Phys. Chem. Lett. 8 (2017) 2700–2704.
[172] J.C. Hill, K.S. Choi, J. Mater. Chem. A Mater. Energy Sustain. 1 (2013) 5006–5014.
[173] Z.X. Cai, F.M. Li, W. Xu, Y.Q. Jiang, F. Luo, Y. Wang, X. Chen, Nano Energy 26 (2016) 257–266.
[174] Z.H. Zhu, P. Sarker, C.Q. Zhao, L. Zhou, R.L. Grimm, M.N. Huda, P.M. Rao, ACS Appl. Mater. Inter. 9 (2017) 1459–1470.
[175] F.F. Abdi, A. Chemseddine, S.P. Berglund, R. Krol, J. Phys. Chem. C 121 (2016) 153–160.
[176] J. Zhu, W.Z. Li, J. Li, Y.M. Li, H.S. Hua, Y.H. Yang, Electrochim. Acta 112 (2013) 191–198.
[177] K.C. Leonard, K.M. Nam, H.C. Lee, S.H. Kang, H.S. Park, A.J. Bard, J. Phys. Chem. C 117 (2013) 15901–15910.
[178] W.N. Xu, C.H. Zheng, H. Hua, Q. Yang, L. Chen, Y. Xi, C.G. Hu, Appl. Surf. Sci. 327 (2015) 140–148.
[179] D. Kang, Y. Park, J.C. Hill, K.S. Choi, J. Phys. Chem. Lett. 17 (2014) 2994–2999.
[180] K.J. McDonald, K.S. Choi, Chem. Mater. 23 (2011) 4863–4869.
[181] T.W. Kim, K.S. Choi, J. Phys. Chem. Lett. 7 (2016) 447–451.
[182] Y. Hou, X.Y. Li, Q.D. Zhao, X. Quan, G.H. Chen, Adv. Funct. Mater. 20 (2010) 2165–2174.
[183] A. Sheikh, A. Yengantiwar, M. Deo, S. Kelkar, S. Ogale, Small 9 (2013) 2091–2096.
[184] J.H. Kim, J.H. Kim, J.W. Jang, J.Y. Kim, S.H. Choi, G. Magesh, J. Lee, J.S. Lee,Adv. Energy Mater. (2014), 1401933.
[185] H. Kato, A. Kudo, J. Phys. Chem. B 106 (2002) 5029–5034.
[186] X.G. Shi, H. Yang, Z.X. Liang, A. Tian, X.X. Xue,Nanotechnology 29 (2018), 385605.
[187] K. Yoshimatsu, H. Mashiko, N. Umezawa, K. Horiba, H. Kumigashira, A. Ohtomo, J. Phys. Chem. C 121 (2017) 18717–18724.
[188] J. Boltersdorf, I. Sullivan, T.L. Shelton, Z. Wu, M. Gray, B. Zoellner, F.E. Osterloh, P.A. Maggard, Chem. Mater. Chem. Mater. 28 (2016) 8876–8889.
[189] K. Wu, C.T. Liu, S.M. Wei, Q.Q. Zhu, F.D. Li, ECS Trans. 53 (2013) 49–56.
[190] J. Song, T.L. Kim, J. Lee, S.Y. Cho, J. Cha, S.Y. Jeong, H. An, W. Kim, Y. Jung, J. Park, G.Y. Jung, D. Kim, J.Y. Jo, S.D. Bu, H.W. Jang, S. Lee, Nano Res. 11 (2018) 642–655.
[191] B.N. Kim, G. Seo, S.W. Huang, H. Yu, B. Ahn, H. Seo, I.S. Cho, Ceram. Int. 44 (2018) 1843–1849.
[192] K. Iwashina, A. Kudo, J. Am. Chem. Soc. 133 (2011) 13272–13275.
[193] C.G. Read, Y. Park, K.S. Choi, J. Phys. Chem. Lett. 3 (2012) 1872–1876.
[194] M.S. Prevot, N. Guijarro, K. Sivula, ChemSusChem 8 (2014) 1359–1367.
[195] Y.J. Jang, Y.B. Park, H.E. Kim, Y.H. Choi, H.C. Sun, J.S. Lee, Chem. Mater. 28 (2016) 6054–6061.
[196] N.T. Hahn, V.C. Holmberg, B.A. Korgel, C.B. Mullins, J. Phys. Chem C 116 (2012) 6459–6466.
[197] S.P. Berglund, F.F. Abdi, P. Bogdanoff, A. Chemseddine, D. Friedrich, R. Krol, Chem. Mater. 28 (2016) 4231–4242.
[198] S.P. Berglund, H.C. Lee, P.D. Nuñez, A.J. Bard, C.B. Mullins, Phys. Chem. Chem. Phys. 15 (2013) 4554–4565.
[199] D. Kang, J.C. Hill, Yl. Park, K.S. Choi, Chem. Mater. 28 (2016) 4331–4340.
[200] F. Wang, W. Septina, A. Chemseddine, F.F. Abdi, D. Friedrich, P. Bogdanoff, R. Krol, S.D. Tilley, S.P. Berglund, J. Am. Chem. Soc. 139 (2017) 15094–15103.
[201] J.E. Park, Y. Hu, J.W. Krizan, Q.D. Gibson, U.T. Tayvah, A. Selloni, R.J. Cava, A.B. Bocarsly, Chem. Mater. 30 (2018) 2574–2582.
[202] X. Li, A.J. Liu, D.M. Chu, C.Y. Zhang, Y.K. Du, J. Huang, P. Yang, Catalysts 8 (2018) 1–10.
[203] I. Shintaro, Y. Keisuke, M. Takuya, H. Hidehisa, M. Yasumichi, I. Tatsumi, J. Am. Chem. Soc. 132 (2010) 17343–17345.
[204] G. Rekhila, Y. Bessekhouad, M. Trari, Int. J. Hydrogen Energy 38 (2013) 6335–6343.
[205] U.A. Joshi, A.M. Palasyuk, P.A. Maggard, J. Phys. Chem. C 115 (2011) 13534–13539.
[206] A.K. Díaz-Garcíaa, T. Lana-Villarreala, R. Gómeza, J. Mater. Chem. A Mater. Energy Sustain. 3 (2015) 19683–19687.
[207] J. Gu, Y. Yan, J.W. Krizan, Q.D. Gibson, Z.M. Detweiler, R.J. Cava, A.B. Bocarsly, J. Am. Chem. Soc. 136 (2014) 830–833.
[208] M. Trari, A. Bouguelia, Y. Bessekhouad, Sol. Energy Mater. Sol. Cells 90 (2006) 190–202.
[209] H.C. Isaac, F.S. Francisco, A. Renaudb, J.L. Beatriz, O. Fabrice, C. Laurent, S. Jobicc, G. Sixto, Electrochim. Acta 113 (2013) 570–574.
[210] B. Bellal, B. Hadjarab, N. Benreguia, Y. Bessekhouad, M. Trari, J. Appl. Electrochem. 41 (2011) 867–872.
[211] K.M. Nam, H.S. Park, H.C. Lee, B.H. Meekins, K.C. Leonard, A.J. Bard, J. Phys. Chem. Lett. 4 (2013) 2707–2710.
[212] C.M. Jiang, G. Segev, L.H. Hess, G. Liu, G. Zaborski, F.M. Toma, J.K. Cooper, I.D. Sharp, ACS Appl. Mater. Inter. 10 (2018) 10627–10633.
[213] D. Tang, A.J.E. Rettie, O. Mabayoje, B.R. Wygant, Y.Q. Lai, Y.X. Liu, C.B. Mullins, J. Mater. Chem. A Mater. Energy Sustain. 4 (2016) 3034–3042.
[214] D. Tang, O. Mabayoje, Y.Q. Lai, Y.X. Liu, C.B. Mullins, J. Electrochem. Soc. 164 (2017) H299–H306.
[215] N.S. Lewis, D.G. Nocera, Proc. Natl. Acad. Sci. U. S. A. 103 (2006) 15729–15735.
[216] C.C.L. McCrory, S. Jung, I.M. Ferrer, S.M. Chatman, J.C. Peters, T.F. Jaramillo, J. Am. Chem. Soc. 137 (2015) 4347–4357.
[217] F. Di Quarto, V. Figà, P. Bocchetta, M. Santamaria, Electrochem. Solid-State Lett. 10 (2007) H305–H308.

[218] P. Wang, T. Minegishi, G. Ma, K. Takanabe, Y. Satou, S. Maekawa, Y. Kobori, J. Kubota, K. Domen, J. Am. Chem. Soc. 134 (2012) 2469–2472.
[219] J.J. Bozell, G.R. Petersen, Green Chem. 12 (2010) 539–554.
[220] S.E. Davis, L.R. Houk, E.C. Tamargo, A.K. Datye, R.J. Davis, Catal. Today 160 (2011) 55–60.
[221] G. Grabowski, J. Lewkowski, R. Skowroński, Electrochim. Acta 36 (1991) 1995.
[222] K.R. Vuyyuru, P. Strasser, Catal. Today 195 (2012) 144–154.
[223] H.G. Cha, K.S. Choi, Nat. Chem. 7 (2015) 328–333.
[224] H. He, J. Du, B. Wu, X. Duan, Y. Zhou, G. Ke, T. Huo, Q. Ren, L. Bian, F. Dong, Green Chem. 20 (2018) 3722–3726.
[225] A. Hammerl, M.A. Hiskey, G. Holl, T.M. Klapötke, K. Polborn, J. Stierstorfer, J.J. Weigand, Chem. Mater. 17 (2005) 3784–3793.
[226] T. Li, T. Kasahara, J. He, K.E. Dettelbach, G.M. Sammis, C.P. Berlinguette, Nat. Commun. 8 (2017) 390.
[227] H. Tateno, Y. Miseki, K. Sayama, Chem. Commun. (Camb.) 53 (2017) 4378–4381.
[228] L.C. Bai, F. Li, Y. Wang, H. Li, X.J. Jiang, L.C. Sun, Chem. Commun. (Camb.) 52 (2016) 9711–9714.
[229] R. Zhang, M. Shao, Z. Li, F. Ning, M. Wei, D.G. Evans, X. Duan, Chem. Eur. J. 23 (2017) 8142–8147.
[230] M. Rafiee, K.C. Miles, S.S. Stahl, J. Am. Chem. Soc. 137 (2015) 14751–14757.
[231] J.Y. Becker, D. Zemach, J. Chem. Soc. Perkin Trans. I 2 (1981) 336–340.
[232] S. Kamimuraa, Y. Kuboa, T. Tsubotaa, T. Ohnoa, Appl. Catal. B-Environ. 225 (2018) 445–451.
[233] H. Tateno, S. Iguchi, Y. Miseki, K. Sayama, Angew. Chem. Int. Ed. 57 (2018) 11238–11241.

Huichao He studied at Chongqing University and received his Ph. D in chemical engineering and technology in Dec. 2014. Dr. He was a visiting student at the University of Texas at Austin (USA) from Sept. 2012 to Feb. 2014. In 2015, Dr. He joined as an assistant professor of the State Key Laboratory of Environmental-Friendly Energy Materials, School of Materials Science and Engineering, Southwest University of Science and Technology (China). His research currently focuses on the ternary metal oxide photoelectrodes for solar water splitting and organic synthesis.

Aizhen Liao is a Ph.D student in physics at the Nanjing University under the supervision of Professors Zhigang Zou and Yong Zhou. Her research interests focus on photoelectrochemical water splitting.

Wenlong Guo received his Ph. D in chemical engineering and technology from Chongqing University in July 2017. During Sept. 2014 to Sept. 2016, Dr. Guo was a visiting student at the University of Texas at Austin (USA). In 2017, Dr. Guo joined the College of Chemistry of Chongqing Normal University (China) as an assistant professor. His research currently focuses on the preparation of ternary metal oxide photoelectrodes and their application in solar water splitting.

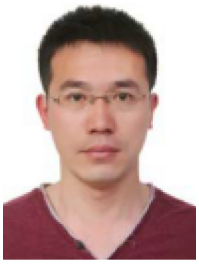

Wenjun Luo is Associate Professor at College of Engineering and Applied Sciences, Nanjing University, China. He received his Ph.D degree from Department of Materials Science and Engineering at Nanjing University in Dec. 2008. And then, he worked at Eco-materials and Renewable Energy Research Center, Nanjing University as a postdoc and a research scientist for the next six years. He joined the faculty of Institute of Advanced Materials (IAM), Nanjing Tech University in Nov. 2014 and moved to College of Engineering and Applied Sciences, Nanjing University as an Associate Professor in Oct. 2018. His current research interests include photoelectrochemistry for solar energy conversion and storage, such as solar water splitting, CO_2 reduction and solar rechargeable devices.

Yong Zhou studied chemistry and physics at the University of Science and Technology of China (USTC) and received his Ph.D there in 2000. After working at Kyoto University in 2000–01, the Max Planck Institute of Colloids and Interfaces in 2002–03, the National Institute of Materials Science (NIMS, Japan) in 2003–04, the National Institute of Advanced Industrial Science and Technology (AIST, Japan) in 2004–08, and the National University of Singapore (NUS) in 2008–09, he joined as a full professor of the Eco-materials and Renewable Energy Research Center (ERERC), School of Physics, National Laboratory of Solid State Microstructures, Nanjing University (China). His research currently focuses on the design and fabrication of solar-light driven clean energy materials for photocatalysis and solar cells.

Zhigang Zou received his bachelor's and master's degrees from Tianjing University (China) in 1982 and 1986, respectively. He was a lecturer at Tianjing University from September 1986 to March 1991. Then, he moved to the Research Laboratory of Engineering Materials at the Tokyo Institute of Technology (Japan) and served as a visiting Researcher. After receiving his PhD degree from the University of Tokyo (Japan) in 1996, he was a researcher at the Photoreaction Control Research Center, National Institute of Advanced Industrial Science and Technology (AIST), Japan. He has been with the Department of Physics at Nanjing University (China) as a distinguished professor of the Chang Jiang Scholars Program since 2003. He is also the Director of the Ecomaterials and Renewable Energy Research Center at Nanjing University. His current research interests includephotocatalysis, solar cells, and fuel cells. Prof. Zou was selected as Academician of Chinese Academy of Sciences in 2015